Comput Geosci (2008) 12:541–571
DOI 10.1007/s10596-008-9094-x

ORIGINAL PAPER

Multiphase flow modeling with general boundary conditions and automatic phase-configuration changes using a fractional-flow approach

Heejun Suk · Gour-Tsyh Yeh

Received: 15 January 2008 / Accepted: 2 June 2008 / Published online: 12 July 2008

Abstract The multiphase flow simulator moving particle semi-implicit (MPS) method is developed based on the fractional-flow approach, originated in the petroleum engineering literature, considering the fully three-phase flow with general boundary conditions. The fractional flow approach employs water saturation, total liquid saturation, and total pressure as primary variables. Most existing models based upon fractional flow are limited to two-phase flow and specific boundary conditions. Although there appear a number of three-phase flow models, they were mostly developed using pressure-based approaches, which require variable-switch techniques to deal with phase appearance and disappearance. The use of fractional flow-based approaches in MPS makes it unnecessary to use variable-switching to handle the change of phase configurations because the water saturation, total liquid saturation, and total pressure exist throughout the solution domain regardless of whether certain phases are present or not. Furthermore, most existing fractional flow-based models consider only specific boundary conditions, usually Dirichlet-type pressure for water phase and flux-type boundary for nonaqueous phase liquid or particular combinations for individual phase. However, the present model considers general boundary conditions of ten most possible and plausible cases. The first eight cases are the combinations of the phase pressure or the phase flux of each of the three individual phases. The other two cases are the variable boundary conditions: one for water-medium interface and the other for the air-medium interface when the directions of fluxes are not known a priori. Thus, the model's capabilities of handling general boundary conditions extend the simulators' usefulness in the field system.

Keywords Multiple-phase flow · Fractional flow approach · General boundary conditions · Phase configuration change

H. Suk
Korea Institute of Geosciences and Mineral Resources, DaeJeon, South Korea
e-mail: sxh60@kigam.re.kr

G.-T. Yeh (✉)
Department of Civil and Environmental Engineering, University of Central Florida, 442B/C ENG II, Orlando, FL 32816-2450, USA
e-mail: gyeh@mail.ucf.edu

1 Introduction

Two main approaches have been developed for modeling multi-phase flow, arising in the disciplines of (1) hydrology and (2) petroleum engineering. The first is based on individual balance equations for each of the fluids, whereas the second involves manipulation and combination of those balance equations into modified forms, with concomitant introduction of ancillary functions such as the fractional flow function.

The first approach is referred to as pressure based, whereas the second approach is referred to as fractional based. The pressure-based approach has been widely used in the hydrologic literature. In this approach, the governing equations are written in terms of the pressures through a straightforward substitution of Darcy's equation into the mass balance equations for each phase. The three governing equations are strongly coupled via nonlinear coefficients resulting from the constitutive relationships among phase saturations and

pressures. This approach has been adopted by a number of authors [1, 3, 6, 8, 10, 11, 12, 16, 19].

The fractional-flow approach, originated in the petroleum engineering literature, employs water saturation, total liquid saturation, and a total pressure as the primary variables. In other words, the three transport equations governing the spatial–temporal distribution of three-phase pressures are transformed into a computationally elliptic equation for the total pressure and two hyperbolically dominant transport equations for water and total liquid saturations. Although the two transport equations of saturations are nonlinear and strongly coupled, the elliptic equation of the total pressure is practically linear and can be considered decoupled from the two transport equations. Thus, computationally, instead of solving three strongly coupled nonlinear equations in the pressure-based approach, one solves only two strongly coupled nonlinear equations and one practically decoupled linear equation.

The difficulty in fractional-flow approaches is in the formulation of general boundary conditions. In petroleum reservoirs, where the total flux is often adopted as a boundary condition, fractional flow approach has no difficulty in using this boundary condition. However, in hydrology, boundary conditions are often posed in terms of individual fluid fluxes or pressures. Although pressure-based approaches can easily handle these types of boundary conditions, fractional-flow approaches cannot directly use them to solve the multiphase problem except for a few specific cases. Fractional-flow approaches require that the boundary conditions be posed as the total pressure or total flux for the total-pressure equation, the water saturation or the water flux for the water saturation equation, and the liquid saturation or the liquid flux for the liquid saturation equation. The fractional approach has been employed by several authors [2, 9]. However, until now, most fractional flow approaches have been limited to two phases and specific boundary conditions. Binning and Celia [2], used fractional flow approach with the aim of gaining significant improvement in computational efficiency, but they pointed out that, when generalized boundary conditions are incorporated into a numerical model, there was little or no computational advantage because the fractional flow equation must be coupled with a nonlinear iterative scheme to find the correct boundary conditions. Thus, they considered the only one combination of boundary types, which is a flux type for water phase and Dirichlet type for air phase.

In this study, robust and efficient strategies that may be used to transform iteratively (using an outer iteration loop) general types of boundary conditions found in pressure-based approaches to those required for fractional-flow approaches are researched. As a result, the outer-loop iterations required for the boundary condition types 2 through 4 and 6 through 8 in Table 2 is usually number only two or three. For boundary condition types 1 and 5, there is no need for the outer iteration at all. Furthermore, the number of iterations in the inner loop to solve the coupled nonlinear water and liquid saturation equations is usually small. Therefore, multiphase flow simulator moving particle semi-implicit (MPS) method is a practical simulator to consider general boundary conditions.

Another distinctive feature of this research is the implementation of MPS; MPS can handle phase configuration changes or phase appearance and disappearance in the solution domain without having to make assumptions and use variable switches [19]. As the primary variables in fractional-flow approaches exist throughout the solution domain whether or not the non-wetting phase is present, there is no need to specify a small, fictitious degree of non-wetting saturation where only the wetting phase is present [10, 15, 19]. When the nonaqueous phase liquid (NAPL) is absent in certain subregions, the governing equations for water saturation and liquid saturation automatically degenerate into two identical equations over such regions, which yield the simulation of equality between water saturation and liquid saturation in the subregions.

In this paper, a two-dimensional finite element model of the simultaneous movement of nonaqueous phase liquid, water, and gas with general boundary conditions is developed. The general boundary conditions consist of ten cases, which can be straightforwardly extended to three-dimensional problems [17]. The first eight cases are combinations of two types of boundaries of individual phases: flux-type and Dirichlet-type boundaries. The other two cases are the variable boundary conditions: one for water-medium interface and the other for the air-medium interface when the directions of fluxes are not known a priori. In addition, the general initial conditions are made of eight combinations of two types of initial conditions of individual phases, saturation and pressure. Therefore, no matter which types of initial and boundary conditions are specified among the eight and ten types, respectively, these can be transformed and incorporated into initial and boundary conditions for total pressure, water saturation, and total liquid saturation of the primary variables. The pressure equation is solved to obtain total pressure distribution by using the standard Galerkin finite element method. The total velocity distribution is computed using the calculated total pressure distribution. The upstream finite element method is employed to solve two saturation equations. Two examples are to

be provided to verify the developed model, MPS. To illustrate model's capability of handling general boundary condition, seven examples are presented, and two more examples are simulated to illustrate the automatic adaptation of phase configuration change. Additionally, one example will also be presented to show the model's applicability in the capillary barrier.

2 Governing equations

A multiphase system in a porous media is assumed to be composed of a solid phase and three fluid phases: water, NAPL, and gas. Each of the three phases is treated here with averaged properties of the fluid, although each of the three phases may consist of several components. For simplicity, we consider the case of incompressible fluids. This assumption of incompressibility leads to the simplification of the governing equation for the total pressure. Without the assumption, a time-derivation term charactering the storage effects of fluids will make the governing equation a transient one. The equations for the flow of three fluid phases in a porous medium are given by the conservation of mass:

$$\frac{\partial(\phi\rho_\alpha S_\alpha)}{\partial t} + \nabla \bullet (\rho_\alpha \mathbf{V}_\alpha) = Q_\alpha. \tag{1}$$

where α is the subscript indicating the phase, 1 for water, 2 for NAPL, and 3 for gas, ϕ is the effective porosity of the porous medium, ρ_α is the density of phase α, S_α is the saturation of phase α, $\mathbf{V}_\alpha$ is the Darcy's velocity of phase α, Q_α is a source or sink term of phase α, and t is time. The Darcy's velocity of phase α, $\mathbf{V}_\alpha$, is defined by

$$\mathbf{V}_\alpha = -\frac{k_{r\alpha}\mathbf{k}}{\mu_\alpha}(\nabla P_\alpha + \rho_\alpha g \nabla z), \tag{2}$$

where $\mathbf{k}$ is the intrinsic permeability tensor, $k_{r\alpha}$ is the relative permeability of phase α, μ_α is the dynamic viscosity of the phase α, P_α is the pressure of phase α, g is the gravitational constant, and z is elevation. For the three-phase cases, total velocity, $\mathbf{V}_t$, defined as the sum of the phase velocities is given by

$$\begin{aligned}\mathbf{V}_t &= \mathbf{V}_1 + \mathbf{V}_2 + \mathbf{V}_3 \\ &= -\frac{k_{r1}\mathbf{k}}{\mu_1}(\nabla P_1 + \rho_1 g\nabla z) - \frac{k_{r2}\mathbf{k}}{\mu_2}(\nabla P_2 + \rho_2 g\nabla z) \\ &\quad -\frac{k_{r3}\mathbf{k}}{\mu_3}(\nabla P_3 + \rho_3 g\nabla z),\end{aligned} \tag{3}$$

where $\mathbf{V}_1$, $\mathbf{V}_2$, and $\mathbf{V}_3$ are water, NAPL, and gas phase velocities, respectively. If we manipulate Eq. 3 by defining the total mobility, $\kappa = \mathbf{k}\left(k_{r1}/\mu_1 + k_{r2}/\mu_2 + k_{r3}/\mu_3\right)$, and fractional mobility for phase i, $\kappa_i = k_{ri}/\mu_i / \sum_{j=1}^{3} k_{rj}/\mu_j$, for i = 1, 2, and 3, the total velocity can be rewritten as

$$\begin{aligned}V_t = &-\kappa\left[\left(\frac{\kappa_1+\kappa_2+\kappa_3}{3}\right)\nabla(P_1+P_2+P_3)\right] \\ &-\kappa\left[\left(\frac{\kappa_1-\kappa_2}{3}\right)\nabla(P_1-P_2)+\left(\frac{\kappa_1-\kappa_3}{3}\right)\nabla(P_1-P_3)\right. \\ &\left.+\left(\frac{\kappa_2-\kappa_3}{3}\right)\nabla(P_2-P_3)\right] - \kappa\overline{\rho}g\nabla z,\end{aligned} \tag{4}$$

where $\overline{\rho} = \kappa_1\rho_1 + \kappa_2\rho_2 + \kappa_3\rho_3$ is the mobility-weighted average fluid density. As $\kappa_1 + \kappa_2 + \kappa_3 = 1$, Eq. 4 becomes

$$\begin{aligned}V_t = &-\kappa\left[\frac{1}{3}\nabla(P_1+P_2+P_3)\right] \\ &-\kappa\left[\left(\frac{\kappa_1-\kappa_2}{3}\right)\nabla(P_1-P_2)+\left(\frac{\kappa_1-\kappa_3}{3}\right)\nabla(P_1-P_3)\right. \\ &\left.+\left(\frac{\kappa_2-\kappa_3}{3}\right)\nabla(P_2-P_3)\right] - \kappa\overline{\rho}g\nabla z.\end{aligned} \tag{5}$$

If we define the total pressure, P_t, as

$$\begin{aligned}P_t = &\frac{P_1+P_2+P_3}{3} \\ &+\frac{1}{3}\left(\int_0^{P_1-P_2}(\kappa_1-\kappa_2)\,d\eta + \int_0^{P_1-P_3}(\kappa_1-\kappa_3)\,d\eta\right. \\ &\left.+\int_0^{P_2-P_3}(\kappa_2-\kappa_3)\,d\eta\right),\end{aligned} \tag{6}$$

Eq. 5 becomes

$$\mathbf{V}_t = -\kappa\left[\nabla P_t + \overline{\rho}g\nabla z\right]. \tag{7}$$

Therefore, the pressure equation is obtained as follows:

$$-\nabla \bullet \kappa(\nabla P_t + \overline{\rho}g\nabla z) = Q_1/\rho_1 + Q_2/\rho_2 + Q_3/\rho_3. \tag{8}$$

It should be noted that the derivation of Eq. 8 assumes that all three phases are incompressible. Although the assumption of incompressibility for aqueous and NAPL phases are obviously reasonable, the assumption of incompressibility for the gaseous phase needs an

elaboration. The model is intended for application to physical problems where the time-scale defining gas-phase pressure response to forcing is much shorter than that which defines gas-phase saturation response. For these problems, the gas-phase can then be considered effectively incompressible. It is further noted that Eq. 8 is considered linear, as the total mobility κ is practically independent of the primary variable. Thus, it can practically be decoupled from two transport equations of saturations that are to be derived below.

Through algebraic manipulation of Eq. 2, equations are found for relating the individual phase flux, $\mathbf{V}_1$, $\mathbf{V}_2$, and $\mathbf{V}_3$ to the total flux $\mathbf{V}_t$

$$\mathbf{V}_1 = \kappa_1 \mathbf{V}_t - \kappa_1 \kappa\left(\kappa_2 \nabla P_{C12} + \kappa_3 \nabla P_{C13}\right) - \kappa_1 \kappa\left(\rho_1 g \nabla z - \overline{\rho} g \nabla z\right), \tag{9}$$

$$\mathbf{V}_2 = \kappa_2 \mathbf{V}_t - \kappa_2 \kappa\left(\kappa_1 \nabla P_{C21} + \kappa_3 \nabla P_{C23}\right) - \kappa_2 \kappa\left(\rho_2 g \nabla z - \overline{\rho} g \nabla z\right), \tag{10}$$

$$\mathbf{V}_3 = \kappa_3 \mathbf{V}_t - \kappa_3 \kappa\left(\kappa_1 \nabla P_{C31} + \kappa_2 \nabla P_{C32}\right) - \kappa_3 \kappa\left(\rho_3 g \nabla z - \overline{\rho} g \nabla z\right), \tag{11}$$

where P_{C12} (P_{C21}) is the capillary pressure of water (NAPL) and NAPL (water), P_{C13} (P_{C31}) is the capillary pressure of water (gas) and gas (water), P_{C23} (P_{C32}) is the capillary pressure of NAPL (gas) and gas (NAPL). Substitution of Eqs. 9 and 11 into Eq. 1, while assuming incompressible flow and continuity of total flux, results in the following two saturation equations, respectively:

$$\begin{aligned}
&\frac{\partial \phi S_1}{\partial t} + \mathbf{V}_t \bullet \frac{d\kappa_1}{dS_1} \nabla S_1 \\
&\quad = \nabla \bullet \kappa_1 \kappa \left(\kappa_2 \frac{\partial P_{C12}}{\partial S_1} + \kappa_3 \frac{\partial P_{C13}}{\partial S_1} \right) \nabla S_1 \\
&\qquad + \nabla \bullet \kappa_1 \kappa \left(\kappa_2 \frac{\partial P_{C12}}{\partial S_t} + \kappa_3 \frac{\partial P_{C13}}{\partial S_t} \right) \nabla S_t - \kappa_1 \nabla \bullet \mathbf{V}_t \\
&\qquad + \nabla \bullet \kappa_1 \kappa \left(\rho_1 g \nabla z - \overline{\rho} g \nabla z \right) + \frac{Q_1}{\rho_1}
\end{aligned} \tag{12}$$

$$\begin{aligned}
&-\frac{\partial \phi S_t}{\partial t} + \mathbf{V}_t \bullet \frac{d\kappa_3}{dS_t} \nabla S_t \\
&\quad = \nabla \bullet \kappa_3 \kappa \left(\kappa_2 \frac{\partial P_{C32}}{\partial S_1} + \kappa_1 \frac{\partial P_{C31}}{\partial S_1} \right) \nabla S_1 \\
&\qquad + \nabla \bullet \kappa_3 \kappa \left(\kappa_2 \frac{\partial P_{C32}}{\partial S_t} + \kappa_1 \frac{\partial P_{C31}}{\partial S_t} \right) \nabla S_t - \kappa_3 \nabla \bullet \mathbf{V}_t \\
&\qquad + \nabla \bullet \kappa_3 \kappa \left(\rho_3 g \nabla z - \overline{\rho} g \nabla z \right) + \frac{Q_3}{\rho_3}
\end{aligned} \tag{13}$$

where $S_t = S_1 + S_2$ is a total liquid saturation. Equations 12 and 13 are hyperbolically dominant transport equations under most real world conditions, where the effects of capillary pressures are smaller than the fluid velocities on the whole system. This set of two partial differential equations is nonlinear and strongly coupled through the several constitutive relationships that will be discussed below.

The following relationship is needed to complete the description of multiphase flow through porous media:

$$S_1 + S_2 + S_3 = 1. \tag{14}$$

Relative permeability relationships corresponding to the three-phase van Genuchten model have been derived by Parker et al. [14]. The relationships are given by

$$k_{r1} = \overline{S}_1^{1/2} \left[1 - \left(1 - \overline{S}_1^{1/m} \right)^m \right]^2, \tag{15}$$

$$k_{r2} = \left(\overline{S}_t - \overline{S}_1 \right)^{1/2} \left[\left(1 - \overline{S}_1^{1/m} \right)^m - \left(1 - \overline{S}_t^{1/m} \right)^m \right]^2, \tag{16}$$

$$k_{r3} = \left(1 - \overline{S}_t \right)^{1/2} \left(1 - \overline{S}_t^{1/m} \right)^{2m}, \tag{17}$$

where m is the curve shape parameter, $\overline{S}_1 = (S_1 - S_{1r})/(1 - S_{1r})$; S_{1r} is the irreducible saturations of water phase; $\overline{S}_t = (S_1 + S_2 - S_{1r})/(1 - S_{1r})$. In addition, capillary pressure–saturation relationships in the three-phase system follow the model of Parker et al. [14]. The relationships are as follows:

$$\overline{S}_1 = \left[1 + (\alpha_{21} h_{21})^n \right]^{-m} \quad \text{for} \quad h_{21} > 0, \tag{18}$$

$$\overline{S}_1 = 1 \quad \text{for} \quad h_{21} \le 0, , \tag{19}$$

$$\overline{S}_t = \left[1 + (\alpha_{32} h_{32})^n \right]^{-m} \quad \text{for} \quad h_{32} > 0, \tag{20}$$

$$\overline{S}_t = 1 \quad \text{for} \quad h_{32} \le 0. \tag{21}$$

where h_{21} is the NAPL–water capillary head (cm of water), and h_{32} is the air–NAPL capillary head (cm of water).

2.1 Degeneration of three-phase equation into two-phase or one-phase equations

In the total pressure equation, total pressures, total mobility, and the mobility averaged fluid density could be

defined regardless of any system, such as water–NAPL–air, water–air, water–NAPL, etc., and total pressure equations have the same form regardless of phase configuration. To explain how the governing equations in the saturation equations for a three-phase configuration degenerate into two-phase or one-phase configurations, let us consider the water–NAPL phase, water–air phase, or only water-saturated condition with assumption of no point source and sink without the loss of generality.

First, for the water/air-phase configuration in the solution domain, NAPL-phase mobility is zero, and the water-phase plus air-phase mobilities are equal to 1; i.e., $\kappa_2 = 0$ and $\kappa_1 + \kappa_3 = 1$. Using these facts, governing Eqs. 12 and 13 are degenerated into the following equations:

$$\frac{\partial \phi S_1}{\partial t} + \mathbf{V}_t \bullet \frac{d\kappa_1}{dS_1} \nabla S_1 = \nabla \bullet \kappa_1 \kappa \left(\kappa_3 \frac{\partial P_{C13}}{\partial S_1} \nabla S_1 + \kappa_3 \frac{\partial P_{C13}}{\partial S_t} \nabla S_t + (\rho_1 - \overline{\rho})\, g \nabla z \right), \tag{22}$$

$$-\frac{\partial \phi S_t}{\partial t} + \mathbf{V}_t \bullet \frac{d\kappa_3}{dS_t} \nabla S_t = \nabla \bullet \kappa_3 \kappa \left(\kappa_1 \frac{\partial P_{C31}}{\partial S_1} \nabla S_1 + \kappa_1 \frac{\partial P_{C31}}{\partial S_t} \nabla S_t + (\rho_3 - \overline{\rho})\, g \nabla z \right) \tag{23}$$

As $\kappa_1(S_1) + \kappa_3(S_t) = 1$, the following relation can be obtained in the following equation:

$$\frac{\mathrm{d}\kappa_1(S_1)}{\mathrm{d}S_1} \nabla S_1 + \frac{\mathrm{d}\kappa_3(S_t)}{\mathrm{d}S_t} \nabla S_t = 0. \tag{24}$$

Rearranging Eq. 24,

$$\frac{\mathrm{d}\kappa_1(S_1)}{\mathrm{d}S_1} \nabla S_1 = -\frac{\mathrm{d}\kappa_3(S_t)}{\mathrm{d}S_t} \nabla S_t. \tag{25}$$

As $\overline{\rho} = \kappa_1 \rho_1 + \kappa_3 \rho_3$,

$$(\rho_1 - \overline{\rho})\, g \nabla z = (\rho_1 - \kappa_1 \rho_1 - \kappa_3 \rho_3)\, g \nabla z. \tag{26}$$

Rearranging Eq. 26,

$$(\rho_1 - \overline{\rho})\, \mathrm{g} \nabla \mathrm{z} = \big((1 - \kappa_1)\, \rho_1 - \kappa_3 \rho_3\big) g \nabla z. \tag{27}$$

Finally, Eq. 27 can be rewritten in Eq. 28

$$(\rho_1 - \overline{\rho})\, g \nabla z = \kappa_3\, (\rho_1 - \rho_3)\, g \nabla z. \tag{28}$$

Furthermore,

$$(\rho_3 - \overline{\rho})\, \mathrm{g} \nabla \mathrm{z} = -\kappa_1\, (\rho_1 - \rho_3)\, g \nabla z. \tag{29}$$

Using Eqs. 25 and 28, we can write Eq. 22 as

$$\frac{\partial \phi S_1}{\partial t} = \mathbf{V}_t \bullet \frac{\mathrm{d}\kappa_3}{\mathrm{d}S_t} \nabla S_t + \nabla \bullet \kappa_1 \kappa \left(\kappa_3 \frac{\partial P_{C13}}{\partial S_1} \nabla S_1 + \kappa_3 \frac{\partial P_{C13}}{\partial S_t} \nabla S_t + \kappa_3\, (\rho_1 - \rho_3)\, g \nabla z \right). \tag{30}$$

Similarly, Eq. 23 can be rewritten, using Eq. 29, as

$$-\frac{\partial \phi S_t}{\partial t} = -\mathbf{V}_t \bullet \frac{\mathrm{d}\kappa_3}{\mathrm{d}S_t} \nabla S_t + \nabla \bullet \kappa_3 \kappa \left(\kappa_1 \frac{\partial P_{C31}}{\partial S_1} \nabla S_1 + \kappa_1 \frac{\partial P_{C31}}{\partial S_t} \nabla S_t - \kappa_1\, (\rho_1 - \rho_3)\, g \nabla z \right). \tag{31}$$

Multiplying both sides by -1 and using $P_{C31} = -P_{C13}$, Eq. 31 becomes

$$\frac{\partial \phi S_t}{\partial t} = \mathbf{V}_t \bullet \frac{\mathrm{d}\kappa_3}{\mathrm{d}S_t} \nabla S_t + \nabla \bullet \kappa_3 \kappa \left(\kappa_1 \frac{\partial P_{C13}}{\partial S_1} \nabla S_1 + \kappa_1 \frac{\partial P_{C13}}{\partial S_t} \nabla S_t + \kappa_1\, (\rho_1 - \rho_3)\, g \nabla z \right) \tag{32}$$

Equations 30 and 32 are identical. They would yield identical solutions if the initial and boundary conditions were the same. As NAPL is absent in water–air system, the initial conditions for the water and total liquid would be the same. Similarly, the fluxes for the water and total liquid through boundary would be the same as long as consistent boundary conditions are prescribed. Thus, when the phase configuration is the water–air system, the solution of Eqs. 22 and 23 automatically yields $S_1 = S_t$. For this case, Eq. 8 and either Eq. 30 or 32 become the governing equations for two primary unknowns P_t and S_1 or S_t.

Similarly, in the water-saturated system, water-phase mobility is equal to 1, NAPL-phase and air-phase mobilities are zero, and phase mobility averaged fluid

density is equal to water fluid density. The governing equations thus become the following equations:

$$\frac{\partial \phi S_1}{\partial t} = 0, \tag{33}$$

$$-\frac{\partial \phi S_t}{\partial t} = 0. \tag{34}$$

It is seen that Eqs. 33 and 34 are identical in form. These two equations will have the same solutions if initial conditions are the same. Initially, the system is only water-saturated, and both water saturation and total liquid saturation are equal to one. The solutions of Eqs. 33 and 34 yield $S_1 = 1$ and $S_t = 1$. Equation 8 then becomes the governing equation for primary unknown P_t.

Finally, in the water/NAPL-phase system, the air-phase mobility is zero. Using these facts, the governing Eqs. 12 and 13 become

$$\frac{\partial \phi S_1}{\partial t} + \mathbf{V}_t \bullet \frac{\mathrm{d}\kappa_1}{\mathrm{d}S_1}\nabla S_1 = \nabla \bullet \kappa_1 \mathbf{K}\left(\kappa_2 \frac{\partial P_{C12}}{\partial S_1}\nabla S_1 + \kappa_2 \frac{\partial P_{C12}}{\partial S_t}\nabla S_t + (\rho_1 - \overline{\rho})\, g \nabla z\right), \tag{35}$$

$$-\frac{\partial \phi S_t}{\partial t} = 0. \tag{36}$$

From the capillary pressure–saturation relationship, Eq. 18, $\frac{\partial P_{C12}}{\partial S_t}$ is zero. Therefore, Eqs. 35 and 36 become uncoupled from each other. Initially, the air is not present, the total liquid saturation is equal to one, and water saturation is less than one. For this case, Eq. 36 would yield a solution of $S_t = 1$, and Eqs. 8 and 35 are the two governing equations for the two primary variables P_t and S_1.

As discussed above, the governing equations are automatically degenerated depending on the phase configurations without any assumptions or criteria on phase appearance and disappearance, in contrast with pressure-based approaches, in which once a three-phase system goes to a two-phase system such as water–air system, the NAPL flow equation reduces to the identity 0 = 0 because capacities and relative permeabilities related to NAPL become zero [10]. Therefore, to avoid the problem in a pressure-based formulation, minimum cutoff values of capacities and relative permeabilities related to NAPL phase should be assigned. Similarly, according to Pinder and Abriola [15] who used pressure-based approach, to avoid tracing the NAPL-phase front, initially negligible saturation of NAPL in the whole simulation domain, which may produce inaccuracy in solution, is introduced whether or not the NAPL phase is present. However, in fractional-flow approaches, cases in which gas and NAPL phases are absent in any part of the domain (including the entire domain) at any given time are handled without any explicit assumptions or criteria.

2.2 Initial and boundary conditions

When Eqs. 8, 12, and 13 are supplemented with appropriate boundary conditions, they can be solved for the unknowns, P_t, S_1, and S_t. Initial conditions are normally expressed as combinations of pressure and saturation of each phase based on physics of phase configurations:

$$P_i = P_i(x, z) \quad \text{on} \quad \Omega \quad \text{for} \quad i = 1, 2, \text{ and } 3, \tag{37}$$

or

$$S_i = S_i(x, z) \quad \text{on} \quad \Omega \quad \text{for} \quad i = 1, 2, \text{ and } 3, \tag{38}$$

where Ω indicates the whole simulation domain. Table 1 lists eight types of initial condition. No matter which type of initial condition is specified, they must be transformed into following three primary variables, S_1, S_t, and P_t. The transformation is straightforward using Eqs. 6 and 18 through 21.

Boundary conditions can be written as a combination of two types of boundaries of individual phases, namely flux-type and Dirichlet-type boundaries:

$$P_i = P_{ni}(x_b, z_b, t) \quad \text{on} \quad B_{di}, \tag{39}$$

$$\mathbf{V}_i \bullet \hat{n} = q_{ni}(x_b, z_b, t) \quad \text{on} \quad B_{fi}, \tag{40}$$

where (x_b, z_b) is the spatial coordinate on the boundary, $\hat{n}$ is outward unit vector normal to the boundary, P_{ni} and q_{ni} are the prescribed Dirichlet functional value

Table 1 Eight types of initial condition for multiphase flow simulation

Types	P_1	P_2	P_3	S_1	S_2	S_3
1	X	X	X			
2	X	X				X
3	X		X		X	
4		X	X	X		
5			X	X	X	
6		X		X		X
7	X				X	X
8				X	X	X

X indicates chosen item for initial condition

and flux value of phase i, respectively, and B_{di} and B_{fi} are the Dirichlet and flux boundaries for the ith phase, respectively. Table 2 lists ten types of boundary condition including two variable boundary conditions. Similar to the initial condition, no matter which type of boundary condition is specified, they can be incorporated into boundary condition in terms of water- and air-phase variables because primary variables are water and total liquid saturation, which is equal to one minus air saturation.

For boundary condition type 1, all three-phase fluxes are given. Thus, the total flux, being the sum of all three-phase fluxes, is a known quantity. As total flux on the boundary is given, total pressure equation is solved subject to flux boundary condition. The water saturation equation is solved with the given water flux as the boundary condition, and total liquid saturation is solved with the given air flux. Therefore, boundary conditions in type 1 can be explicitly applied for the total pressure equation, water saturation equation, and total liquid saturation without any need for nonlinear iterations. Similarly, for type 5, all three-phase pressures are given; the water saturation and total liquid saturation are explicitly calculated from capillary pressure–saturation relationships in Eqs. 18 through 21. Total pressure on the boundary is calculated from the given three-phase pressures by using Eq. 6. Thus, boundary conditions of type 5 become Dirichlet-type boundary conditions for total pressure, water saturation, and total liquid saturation equations.

However, boundary values of the other six types excluding types 1 and 5 are not explicitly specified in terms of water- and air-phase variables. These boundary values should be estimated from capillary pressure–saturation relationships in Eqs. 18 through 21, 9, 10, and 11 relating individual phase flux to total flux and the total pressure function in Eq. 6. These values need to be iterated until convergent solutions are obtained. For type 2, water-phase flux, NAPL-phase flux, and air pressure are given. The unknown NAPL-phase pressure and water-phase pressure are estimated from the previous known water saturation and total liquid saturation by using the capillary pressure–saturation relationships in Eqs. 18 through 21. The given air pressure, the estimated water pressure and NAPL pressures above are used to calculate the estimated total pressure using the total pressure function, Eq. 6. The estimated total pressure is used as a Dirichlet-type pressure boundary condition for solving total pressure equation. After solving the total pressure equation, the total flux is obtained, and the air flux is estimated by subtracting the given water and NAPL fluxes from the total flux. The estimated air flux is reused as the boundary condition for the total liquid saturation equation. The water saturation equation is directly solved through using the given water-phase flux as the boundary condition. As the boundary values for the total pressure Eq. 8 and total liquid saturation Eq. 13, respectively, are estimated values, they need to be iterated until three primary variables are within the specified error. Thus, it turns out that two iteration loops such as inner and outer iteration loops are needed for solving Eqs. 8, 12, and 13. An inner iteration loop is needed for solving the two nonlinear saturation equations. An outer iteration loop is needed due to estimated nonlinear boundary condition.

In type 3, where water-phase flux, air-phase flux, and NAPL pressure are given on the boundaries, a procedure (differing little from that used for type 2) is used to solve all three equations of the system. First of all, as in type 2, the estimated total pressure is calculated from the given NAPL pressure and estimated water and air pressure that are obtained from the capillary pressure–saturation relations, Eqs. 18 through 21, using

Table 2 Ten types of boundary condition for multiphase flow simulation

Types	P_1	P_2	P_3	$\mathbf{n}\bullet\mathbf{V}_1$	$\mathbf{n}\bullet\mathbf{V}_2$	$\mathbf{n}\bullet\mathbf{V}_3$
1				X	X	X
2			X	X	X	
3		X		X		X
4	X				X	X
5	X	X	X			
6	X	X				X
7	X		X		X	
8		X	X	X		
9	P_1 is specified $\Delta N_1 = 0$ if $\mathbf{n}\bullet\mathbf{V}_2 > 0$ or $\mathbf{n}\bullet\mathbf{V}_2 = 0$ if $\mathbf{n}\bullet\mathbf{V}_2 \le 0$ $\Delta N_3 = 0$ if $\mathbf{n}\bullet\mathbf{V}_3 > 0$ or $\mathbf{n}\bullet\mathbf{V}_3 = 0$ if $\mathbf{n}\bullet\mathbf{V}_3 \le 0$					
10	P_3 is specified $\Delta N_1 = 0$ if $\mathbf{n}\bullet\mathbf{V}_1 > 0$ or $\mathbf{n}\bullet\mathbf{V}_1 = 0$ if $\mathbf{n}\bullet\mathbf{V}_1 \le 0$ $\Delta N_2 = 0$ if $\mathbf{n}\bullet\mathbf{V}_2 > 0$ or $\mathbf{n}\bullet\mathbf{V}_2 = 0$ if $\mathbf{n}\bullet\mathbf{V}_2 \le 0$					

X indicates chosen item for specifying boundary condition

the previous known water saturation and total liquid saturation. The estimated total pressure is then used as a Dirichlet boundary condition for solving the total pressure equation. The water-saturation and total-liquid-saturation equations, respectively, are solved directly using the given water-phase and air-phase fluxes, respectively, as the boundary condition. Thus, for type 3, the boundary values that need iteration are those for the total pressure equation. Therefore, the need for outer iteration is almost eliminated.

In type 4, water pressure and NAPL-phase and air-phase fluxes are given, the total pressure is estimated from the given water pressure and guessed water and total liquid saturations. This estimated total pressure serves as a Dirichlet-type boundary for solving the total pressure equation, from which the total flux on the boundary can be computed. As with type 2, the total liquid saturation equation is directly solved using the given air-phase flux as a flux boundary condition. However, for solving the water saturation equation, the water-phase flux is estimated from the two given fluxes and computed total flux using Eqs. 9 through 11. Therefore, two iteration loops are needed for solving all equations of the system. An outer iteration loop is needed due to estimated nonlinear boundary values, whereas an inner iteration loop is needed for solving the set of simultaneous equations of two nonlinear saturation Eqs. 12 and 13.

In type 6, water and NAPL pressures and air-phase flux are given, air-phase pressure is estimated from capillary pressure–saturation relationships, Eqs. 20 and 21, by using the known total liquid saturation at the previous time step. The two given pressures and the one estimated pressure are used for calculating total pressure using Eq. 6. The estimated total pressure is employed as a Dirichlet-type boundary condition for total pressure equation. In contrast to types 2, 3, and 4, water saturation equation is solved directly by using the calculated water saturation as a Dirichlet-type boundary condition, which is obtained explicitly from two known phase pressures by using the capillary pressure–saturation relationships Eqs. 18 and 19. As air-phase flux is given in type 6, total liquid saturation equation is directly solved by using the given air-phase flux as a flux boundary condition. Similar to type 3, the only estimated nonlinear boundary value is total pressure, but is very weakly dependent on water and total liquid saturations. Therefore, the need for outer iteration is almost eliminated.

In type 8, NAPL-phase and air-phase pressures and water-phase flux are given, the total pressure is estimated, which serves as the Dirichlet-type boundary condition for the total pressure equation. Similar to type 6, water saturation equation is directly solved by using the given water-phase flux as the boundary condition, whereas total liquid saturation is directly solved by using the calculated total liquid saturation as a Dirichlet-type boundary condition, which is obtained explicitly from the two given NAPL-phase and air-phase pressures using the capillary pressure–saturation relationships, Eqs. 20 and 21. As with type 6, the need for outer iteration is almost eliminated.

In type 7, water and air-phase pressures and NAPL flux are given. NAPL pressure can be estimated from capillary pressure–saturation relationship with the iterated value of water saturation. With three-phase pressures known (water and air pressures given and NAPL pressured iterated), the total pressure computed with Eq. 6 serves as a Dirichlet-type condition for the total pressure equation. Thus, total pressure distribution and total flux at the Dirichlet boundary could be obtained. For the water saturation equation, the iterated water saturation equation is used as a Dirichlet-type boundary condition to yield the distribution of water saturation and water flux on the boundary. Similarly, for the total liquid saturation equation, based on the capillary pressure–saturation relationship, the iterated water saturation and given water and air-phase pressures on the boundary are used to compute total liquid saturation as a Dirichlet-type boundary condition to generate the distribution of total liquid saturation and air flux on the boundary. If the iterated water saturation were correct, the sum of the simulated water and air fluxes from the water and total saturation equations must be equal to the difference between the simulated total flux from the pressure equation and given NAPL flux. Thus, the strategies to update the water saturation must ensure this equality. To get the improved iterated water saturation, the differences between the sum of simulated water and air fluxes and simulated total flux minus given NAPL flux need to be calculated using two guessed water saturations at two successive iteration. By linearly interpolating or extrapolating water saturation so that the difference becomes zero, the guessed water saturation can be updated and used as the Dirichlet boundary condition for the next iteration. The process of updating is continued until the changes of all three primary variables between iterations are within specified error tolerance limit.

Different from the above eight types, types 9 and 10 are called variable boundary conditions because directions of fluxes are not known a priori. Specifically, a boundary of type 9 corresponds to water-medium interface, whereas type 10 corresponds to air-medium interface. In type 9, as the water-medium interface is considered, static water pressure is used as the specified

pressure boundary condition for the aqueous phase, whereas the other two pressures are unknown. If flow direction of NAPL flow is into the domain, its normal flux is set to zero, which becomes the Cauchy boundary condition. Otherwise, if flow direction of NAPL is going out, its capillary gradient is set to zero, which becomes the Neumann boundary conditions; that is, the NAPL flows out through the advective processes. Similarly, for the gaseous phase, the boundary condition is specified as either Cauchy or Neumann. Therefore, boundary condition of type 9 has four different cases depending on directions of NAPL and air-phase flows. For all four cases, NAPL phase and air pressures are estimated from the known water saturation and total liquid saturation at the previous time step by using the capillary pressure–saturation relationships, Eqs. 18 through 21. The given water pressure and the estimated NAPL pressure and air pressure above are used to calculate the estimated total pressure using the total pressure function, Eq. 6. The estimated total pressure is used as a Dirichlet pressure boundary condition for solving the total pressure equation. After solving the total pressure equation, total flux is obtained. At each iteration, velocities of each phase are calculated so that the direction of each fluid is known. If the direction of each phase is going out, we will use Neumann boundary condition for solving saturation equations. Otherwise, we will use Cauchy boundary condition. Therefore, water and total liquid saturation can be solved using a different boundary condition for each iteration. If the solution does not converge, iteration will be performed again. Similarly, the next iteration will be performed checking the direction of each phase's velocity.

Similar to type 9, the air-medium interface is considered in type 10; the air pressure is used as a specified pressure boundary condition for the gaseous phase. If the flow directions of water and NAPL phase in type 10 are coming in, their normal fluxes are set to zero, which become Cauchy boundary conditions of saturation equations. If, however, the flow directions of water and NAPL phases are going out, their capillary gradients are set to zero, which become Neumann boundary conditions. As with type 9, it has four different cases depending on the directions of water- and NAPL-phase flows in Type 10. For all four cases, water and NAPL-phase pressures are estimated from the previous known water saturation and total liquid saturation using the capillary pressure–saturation relationships, Eqs. 18 through 21. The given air pressure and the estimated water pressure and NAPL pressure above are used to calculate the estimated total pressure using the total pressure function, Eq. 6. The estimated total pressure is used as a Dirichlet pressure boundary condition for solving total pressure equation. After solving the total pressure equation, total flux is obtained. At each iteration, velocities of each phase are calculated to know the direction of each phase fluid. If the direction of each phase is going out, we will use Neumann boundary condition for solving the saturation equation. Otherwise, we will use Cauchy boundary condition. Therefore, as with type 9, water and total liquid saturations can be solved using different boundary conditions for each iteration. If the solution does not converge, iteration will be performed again. Similar to type 9, the next iteration will be performed with attention to the direction of each phase's velocity.

3 Numerical formulation of multiphase flow in fractional-flow approaches

The pressure equation is solved by using the standard Galerkin finite element method to obtain total pressure at every node. Similarly, total velocity distribution is solved by employing the finite element method using the calculated total pressure at every node. Then, the upstream finite element method with optimized weighting parameters [5, 7] is employed to solve two saturation equations, Eqs. 12 and 13. The two saturation equations are discretized as follows (for finite element applications to subsurface flow, refer to [22, 23]):

$$\left[C_1\right]\left\{\frac{\partial S_1}{\partial t}\right\}+\left[ADW_1\right]\{S_1\}+\left[ADT_1\right]\{S_t\} + [DD_1]\{S_1\}+[E_1]\{S_t\}+[WW_1]\{S_1\}=\{f_1\}, \tag{41}$$

$$\left[C_2\right]\left\{\frac{\partial S_t}{\partial t}\right\}+\left[ADW_2\right]\{S_1\}+\left[ADT_2\right]\{S_t\} + [DD_2]\{S_1\}+[E_2]\{S_t\}+[WW_2]\{S_t\}=\{f_2\}, \tag{42}$$

where

$$\left[C_1\right]_{i,j}=\left[C_2\right]_{i,j}=\int_\Omega \phi N_i N_j \mathrm{d}R, \tag{43}$$

$$\left[ADW_1\right]_{i,j}=\int_\Omega W_i\frac{\mathrm{d}\kappa_1}{\mathrm{d}S_1}\mathbf{V}_t\bullet\nabla N_j\mathrm{d}R - \int_\Omega W_i\frac{\mathrm{d}\left(\kappa_1\kappa g\left(\rho_1-\overline{\rho}\right)\right)}{\mathrm{d}S_1}\nabla z\bullet\nabla N_j\mathrm{d}R, \tag{44}$$

$$\left[ADW_2\right]_{i,j} = \int_{\Omega} W_i \frac{\mathrm{d}\left(\kappa_3 \kappa \left(\rho_3 - \overline{\rho}\right) g\right)}{\mathrm{d}S_1} \nabla z \bullet \nabla N_j \mathrm{d}R, \tag{45}$$

$$\left[ADT_1\right]_{i,j} = -\int_{\Omega} W_i \frac{\mathrm{d}\left(\kappa_1 \kappa g \left(\rho_1 - \overline{\rho}\right)\right)}{\mathrm{d}S_t} \nabla z \bullet \nabla N_j \mathrm{d}R, \tag{46}$$

$$\begin{aligned}\left[ADT_2\right]_{i,j} = &-\int_{\Omega} W_i \frac{\mathrm{d}\kappa_3}{\mathrm{d}S_t} \mathbf{V}_t \bullet \nabla N_j \mathrm{d}R \\ &+ \int_{\Omega} W_i \frac{\mathrm{d}\left(\kappa_3 \kappa \left(\rho_3 - \overline{\rho}\right) g\right)}{\mathrm{d}S_t} \nabla z \bullet \nabla N_j \mathrm{d}R,\end{aligned} \tag{47}$$

$$\left[DD_1\right]_{i,j} = \int_{\Omega} \kappa_1 \kappa (1 - \kappa_1) \frac{\mathrm{d}P_{c12}}{\mathrm{d}S_1} \nabla N_i \bullet \nabla N_j \mathrm{d}R, \tag{48}$$

$$\left[DD_2\right]_{i,j} = \int_{\Omega} \kappa_3 \kappa \kappa_1 \frac{\mathrm{d}P_{c12}}{\mathrm{d}S_1} \nabla N_i \bullet \nabla N_j \mathrm{d}R, \tag{49}$$

$$\left[E_1\right]_{i,j} = \int_{\Omega} \kappa_1 \kappa \kappa_3 \frac{\mathrm{d}P_{c23}}{\mathrm{d}S_t} \nabla N_i \bullet \nabla N_j \mathrm{d}R, \tag{50}$$

$$\left[E_2\right]_{i,j} = \int_{\Omega} \kappa_3 \kappa \left(1 - \kappa_3\right) \frac{\mathrm{d}P_{c23}}{\mathrm{d}S_t} \nabla N_i \bullet \nabla N_j \mathrm{d}R, \tag{51}$$

$$\left[WW_1\right]_{i,j} = \int_{\Omega} N_i \left(\frac{\kappa_1 \nabla \bullet \mathbf{V}_t - Q_1/\rho_1}{S_1}\right) N_j \mathrm{d}R, \tag{52}$$

$$\left[WW_2\right]_{i,j} = \int_{\Omega} N_i \left(\frac{-\kappa_3 \nabla \bullet \mathbf{V}_t + Q_3/\rho_3}{S_t}\right) N_j \mathrm{d}R, \tag{53}$$

$$\begin{aligned}\left\{f_1\right\}_i = &\int_B N_i \kappa_1 \mathbf{V}_t \bullet \hat{n} \mathrm{d}B \\ &- \int_B N_i \mathbf{V}_1 \bullet \hat{n} \mathrm{d}B - \int_B N_i \kappa_1 \kappa \left(\rho_1 - \overline{\rho}\right) g \nabla z \bullet \hat{n} \mathrm{d}B,\end{aligned} \tag{54}$$

and

$$\begin{aligned}\left\{f_2\right\}_i = &-\int_B N_i \kappa_3 \mathbf{V}_t \bullet \hat{n} \mathrm{d}B + \int_B N_i \mathbf{V}_3 \bullet \hat{n} \mathrm{d}B \\ &+ \int_B N_i \kappa_3 \kappa \left(\rho_3 - \overline{\rho}\right) g \nabla z \bullet \hat{n} \mathrm{d}B,\end{aligned} \tag{55}$$

where W_i is the weighting function, N_i is the Galerkin interpolation function, and B indicates boundary. Finally, if we assemble discretized Eqs. 41 and 42, a simultaneous solution set is obtained in the following:

$$\begin{aligned}&\begin{bmatrix} C_1 & 0 \\ 0 & C_2 \end{bmatrix} \begin{Bmatrix} \dfrac{\partial S_1}{\partial t} \\ \dfrac{\partial S_t}{\partial t} \end{Bmatrix} \\ &+ \begin{bmatrix} DD_1 + ADW_1 + WW_1 & E_1 + ADT_1 \\ DD_2 + ADW_1 & E_2 + ADT_2 + WW_2 \end{bmatrix} \\ &\times \begin{Bmatrix} S_1 \\ S_t \end{Bmatrix} = \begin{Bmatrix} f_1 \\ f_2 \end{Bmatrix}.\end{aligned} \tag{56}$$

3.1 Degeneration of three-phase equation into two-phase or one-phase equations

To explain how the numerical formulations are degenerated depending on the phase configuration, we consider three different phase configurations with assumption of no source and sink: water/NAPL-phase system, water/air-phase system, and only water-only saturated system. First, in the water/air-phase system, numerical formulation could be indicated as following:

$$\left[C_1\right] \left\{\frac{\partial S_1}{\partial t}\right\} + \left[ADW_1\right] \left\{S_1\right\} + \left[DD_1\right] \left\{S_1\right\} = \left\{f_1\right\}, \tag{57}$$

$$\left[C_2\right] \left\{\frac{\partial S_t}{\partial t}\right\} + \left[ADT_2\right] \left\{S_t\right\} + \left[E_2\right] \left\{S_t\right\} = \left\{f_2\right\}, \tag{58}$$

where

$$\left[C_1\right]_{i,j} = \left[C_2\right]_{i,j} = \int_{\Omega} \phi N_i N_j \mathrm{d}R, \tag{59}$$

$$\begin{aligned}\left[ADW_1\right]_{i,j} = &\int_{\Omega} W_i \frac{\mathrm{d}\kappa_1}{\mathrm{d}S_1} \mathbf{V}_t \bullet \nabla N_j \mathrm{d}R \\ &- \int_{\Omega} W_i \frac{\mathrm{d}\left(\kappa_1 \kappa g \left(\rho_1 - \overline{\rho}\right)\right)}{\mathrm{d}S_1} \nabla z \bullet \nabla N_j \mathrm{d}R,\end{aligned} \tag{60}$$

$$[ADT_2]_{i,j} = -\int_\Omega W_i \frac{\mathrm{d}\kappa_3}{\mathrm{d}S_t}\mathbf{V}_t \bullet \nabla N_j \mathrm{d}R + \int_\Omega W_i \frac{\mathrm{d}\left(\kappa_3 \kappa g\left(\rho_3 - \overline{\rho}\right)\right)}{\mathrm{d}S_t}\nabla z \bullet \nabla N_j \mathrm{d}R, \tag{61}$$

$$[DD_1]_{i,j} = \int_\Omega \kappa_1 \kappa\left(1-\kappa_1\right)\frac{\mathrm{d}P_{c12}}{\mathrm{d}S_1}\nabla N_i \bullet \nabla N_j \mathrm{d}R, \tag{62}$$

$$[E_2]_{i,j} = \int_\Omega \kappa_3 \kappa\left(1-\kappa_3\right)\frac{\mathrm{d}P_{c23}}{\mathrm{d}S_t}\nabla N_i \bullet \nabla N_j \mathrm{d}R, \tag{63}$$

$$\{f_1\}_i = \int_B N_i \kappa_1 \mathbf{V}_t \bullet \hat{n}\mathrm{d}B - \int_B N_i \mathbf{V}_1 \bullet \hat{n}\mathrm{d}B - \int_B N_i \kappa_1 \kappa\left(\rho_1 - \overline{\rho}\right) g\nabla z \bullet \hat{n}\mathrm{d}B, \tag{64}$$

$$\{f_2\}_i = -\int_B N_i \kappa_3 \mathbf{V}_t \bullet \hat{n}\mathrm{d}B + \int_B N_i \mathbf{V}_3 \bullet \hat{n}\mathrm{d}B + \int_B N_i \kappa_3 \kappa\left(\rho_3 - \overline{\rho}\right) g\nabla z \bullet \hat{n}\mathrm{d}B. \tag{65}$$

If we assemble discretized Eqs. 57 and 58, a simultaneous solution set is obtained in the following:

$$\begin{bmatrix} C_1 & 0 \\ 0 & C_2 \end{bmatrix}\begin{Bmatrix} \dfrac{\partial S_1}{\partial t} \\ \dfrac{\partial S_t}{\partial t} \end{Bmatrix} + \begin{bmatrix} DD_1 + ADW_1 & 0 \\ 0 & E_2 + ADT_2 \end{bmatrix}\begin{Bmatrix} S_1 \\ S_t \end{Bmatrix} = \begin{Bmatrix} f_1 \\ f_2 \end{Bmatrix}. \tag{66}$$

In the water–NAPL system, the discretization is as following:

$$[C_1]\left\{\frac{\partial S_1}{\partial t}\right\} + [ADW_1]\{S_1\} + [DD_1]\{S_1\} = \{f_1\}, \tag{67}$$

$$[C_2]\left\{\frac{\partial S_t}{\partial t}\right\} = \{f_2\}, \tag{68}$$

where

$$[C_1]_{i,j} = [C_2]_{i,j} = \int_\Omega \phi N_i N_j \mathrm{d}R, \tag{69}$$

$$[ADW_1]_{i,j} = \int_\Omega W_i \frac{\mathrm{d}\kappa_1}{\mathrm{d}S_1}\mathbf{V}_t \bullet \nabla N_j \mathrm{d}R - \int_\Omega W_i \frac{\mathrm{d}\left(\kappa_1 \kappa\left(\rho_1 - \overline{\rho}\right) g\right)}{\mathrm{d}S_1}\nabla z \bullet \nabla N_j \mathrm{d}R, \tag{70}$$

$$[DD_1]_{i,j} = \int_\Omega \kappa_1 \kappa \kappa_2 \frac{\mathrm{d}P_{c12}}{\mathrm{d}S_1}\nabla N_i \bullet \nabla N_j \mathrm{d}R, \tag{71}$$

$$\{f_1\}_i = \int_B N_i \kappa_1 \mathbf{V}_t \bullet \hat{n}\mathrm{d}B - \int_B N_i \mathbf{V}_1 \bullet \hat{n}\mathrm{d}B - \int_B N_i \kappa_1 \kappa\left(\rho_1 - \overline{\rho}\right) g\nabla z \bullet \hat{n}\mathrm{d}B, \tag{72}$$

$$\{f_2\}_i = \int_B N_i \mathbf{V}_3 \bullet \hat{n}\mathrm{d}B, \tag{73}$$

As in the previous case, if we assemble discretized Eqs. 67 and 68, a simultaneous solution set is obtained in Eq. 74:

$$\begin{bmatrix} C_1 & 0 \\ 0 & C_2 \end{bmatrix}\begin{Bmatrix} \dfrac{\partial S_1}{\partial t} \\ \dfrac{\partial S_t}{\partial t} \end{Bmatrix} + \begin{bmatrix} DD_1 + ADW_1 & 0 \\ 0 & 0 \end{bmatrix}\begin{Bmatrix} S_1 \\ S_t \end{Bmatrix} = \begin{Bmatrix} f_1 \\ f_2 \end{Bmatrix}. \tag{74}$$

In the water-only saturated system, the numerical formulations are as following:

$$[C_1]\left\{\frac{\partial S_1}{\partial t}\right\} = \{f_1\}, \tag{75}$$

$$[C_2]\left\{\frac{\partial S_t}{\partial t}\right\} = \{f_2\}, \tag{76}$$

where

$$[C_1]_{i,j} = [C_2]_{i,j} = \int_\Omega \phi N_i N_j \mathrm{d}R, \tag{77}$$

$$\{f_1\}_i = -\int_B N_i \mathbf{V}_1 \bullet \hat{n}\mathrm{d}B, \tag{78}$$

$$\{f_2\}_i = \int_B N_i \mathbf{V}_3 \bullet \hat{n}\mathrm{d}B. \tag{79}$$

In this system, simultaneous equation set is obtained in Eq. 80 by assembling discretized equations (75) and (76):

$$\begin{bmatrix} C_1 & 0 \\ 0 & C_2 \end{bmatrix} \begin{Bmatrix} \frac{\partial S_1}{\partial t} \\ \frac{\partial S_t}{\partial t} \end{Bmatrix} + \begin{bmatrix} 0 & 0 \\ 0 & 0 \end{bmatrix} \begin{Bmatrix} S_1 \\ S_t \end{Bmatrix} = \begin{Bmatrix} f_1 \\ f_2 \end{Bmatrix} \tag{80}$$

As stated above, numerical formulations are automatically changed based on the phase configuration of water saturation and total liquid saturation, from a three-phase system to a two-phase system (or vice versa) or from a two-phase system to a one-phase system (or vice versa). This means that any phase configurations in the solution domain is systematically handled with the governing equation based on fractional-flow approach without any explicit criterion or assumption whether or not the non-wetting phase is absent in any part of the solution domain.

4 Verification

Two examples are presented to verify the developed model, MPS. The first concerns a water infiltration problem in the homogeneous water-wet vertical soil column. The verification is performed through the comparison of MPS solutions with 2DFATMIC [21]. For comparisons, identical convergence tolerance and time-stepping scheme are used for both MPS and 2DFATMIC. The second example considers simulation of two-phase flow of NAPL and water in a horizontal soil column. In this example, model verification is carried out by comparison to an analytical solution, based on one by McWhorter and Sunada [13].

4.1 Comparison of MPS with 2DFATMIC

This example is selected to represent the simulation of a one-dimensional problem. The conceptualization of the problem is given in terms of initial and boundary conditions, fluid properties, and material properties in Fig. 1. For numerical simulations, the finite element discretization is also given. For this problem, water is applied to the top of a vertical soil column at a constant rate of 10 cm/day for about 70 min. The column is 40 cm long and 1 cm wide. The soil column is assumed to contain soil with an intrinsic permeability of 4.27×10^{-8} cm^2 and a porosity of 0.25. The unsaturated characteristic hydraulic properties of the soil in the column are characterized with a van Genuchten model

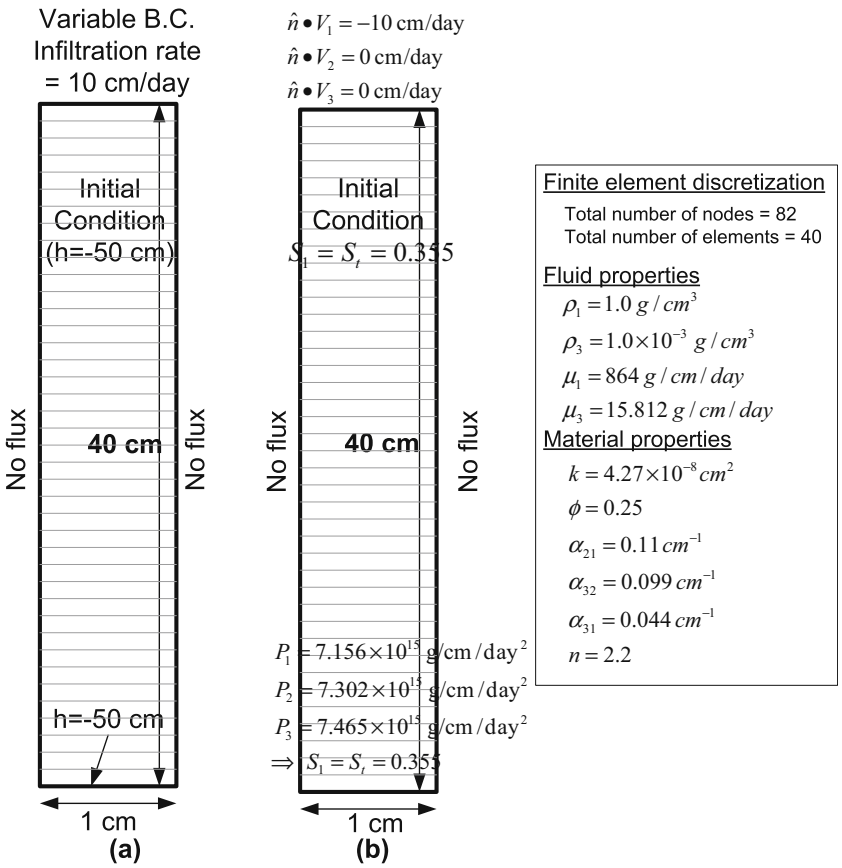

Fig. 1 Problem descriptions for **a** 2DFATMIC and **b** 2DMPS: domain of interest, initial and boundary conditions, fluid properties, material properties, and finite element discretization

[14]. The van Genuchten parameters α_{21}, α_{32}, α_{31}, and n are 0.11, 0.099, 0.044, and 2.2 cm^{-1}, respectively.

4.1.1 Input conditions of 2DFATMIC

The initial conditions are assumed that a pressure head of −50 cm is imposed on the whole domain. The boundary conditions are given as follows: no flux is imposed on the left and right surfaces of the column, pressure head is held at −50 cm on the bottom, and variable condition is used on the top surface of the column with a ponding depth of zero, minimum pressure of −900 cm, and a rainfall of 10 cm/day. The region of interest, i.e., the whole domain, is discretized with $1 \times 40 = 40$ elements with the element size of 1 by 1 cm, resulting in 82 node points. A variable time-step size is used. The initial time-step size is about 4 s and each subsequent time-step size is increased by 0.1 times with a maximum time-step size not greater than 1×10^{-3} day (86.4 s). Simulation time is 70 min. In this study, the chosen numerical scheme is the mass lumping method [22, 23].

4.1.2 Input conditions of MPS

Initial conditions are assumed that water-phase pressure and NAPL pressure is 7.156×10^{15} and 7.302×10^{15} g cm^{-1} day^{-2}, and gas phase pressure is 7.465×10^{15} g cm^{-1} day^{-2}, which is equal to atmospheric pressure, in the whole region (initial condition type 1 in Table 1). The boundary conditions are given as follows. No flux of any of the three phases is imposed on the left and right surfaces of the column. Pressures of three phases are held at 7.156×10^{15} g cm^{-1} day^{-2} of water phase, 7.302×10^{15} g cm^{-1} day^{-2} of NAPL phase, and 7.465×10^{15} g cm^{-1} day^{-2} of gas phase on the bottom (boundary condition type 5 in Table 2). The boundary conditions are determined on the consistency with those of 2DFATMIC. In the 2DFATMIC, the water saturation of 0.355, which is equivalent to the pressure head of −50 cm, is used as the Dirichlet boundary condition for bottom boundary condition. Similarly, in the MPS, the boundary conditions are determined using the capillary pressure–saturation relationships, Eqs. 18 through 21, and atmospheric pressure of air. In order to have the water saturation and total liquid saturation of 0.355 on the bottom boundary, NAPL pressure is calculated from atmospheric pressure of air using Eqs. 20 and 21, and water-phase pressure is calculated from the calculated NAPL pressure using Eqs. 18 and 19. Thus, we need to specify three pressures on the bottom boundary, even though two-phase flow (water–air) is simulated. On the top boundary, the flux of water phase is equal to 10 cm/day, but NAPL-phase and air-phase fluxes are equal to zero (boundary condition type 1 in Table 2). The region of interest is discretized same as in 2DFATMIC. Variable time step is used same as in 2DFATMIC. In this study, the chosen numerical schemes are upstream weighting method and lumping method. Figure 2 shows effective water saturation with height at various times. Figure 2 illustrates very good agreement between MPS and 2DFATMIC.

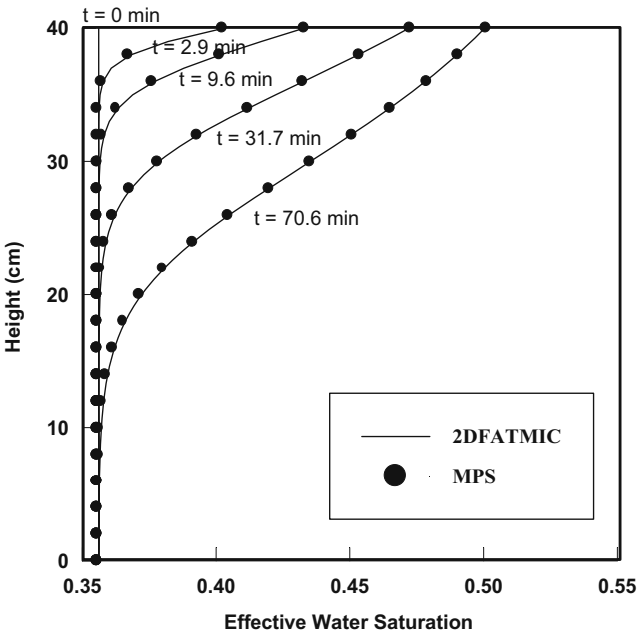

Fig. 2 Comparison of MPS solutions with 2DFATMIC solutions for model verification

4.2 Comparison of MPS solution with exact solution

Figure 3 depicts the conceptual model of this problem in terms of initial and boundary conditions, fluid properties, material properties, and finite element discretization. In general, analytical solutions incorporating fully the effects of gravity and capillarity in transient multiphase flow through heterogeneous porous media are not tractable. Many other authors [2, 20] have chosen to verify their models against the classical Burkley–Leverett problem [4] that represents one dimensional, horizontal two-phase flow in the absence of capillary forces. In this study, model verification is carried out by comparison to an analytical solution, based on one by McWhorter and Sunada [13], which fully incorporates the effect of capillarity. This example demonstrates that general boundary conditions can be handled with fractional flow-based approaches even in the case of capillary-driven flows. The physical scenario

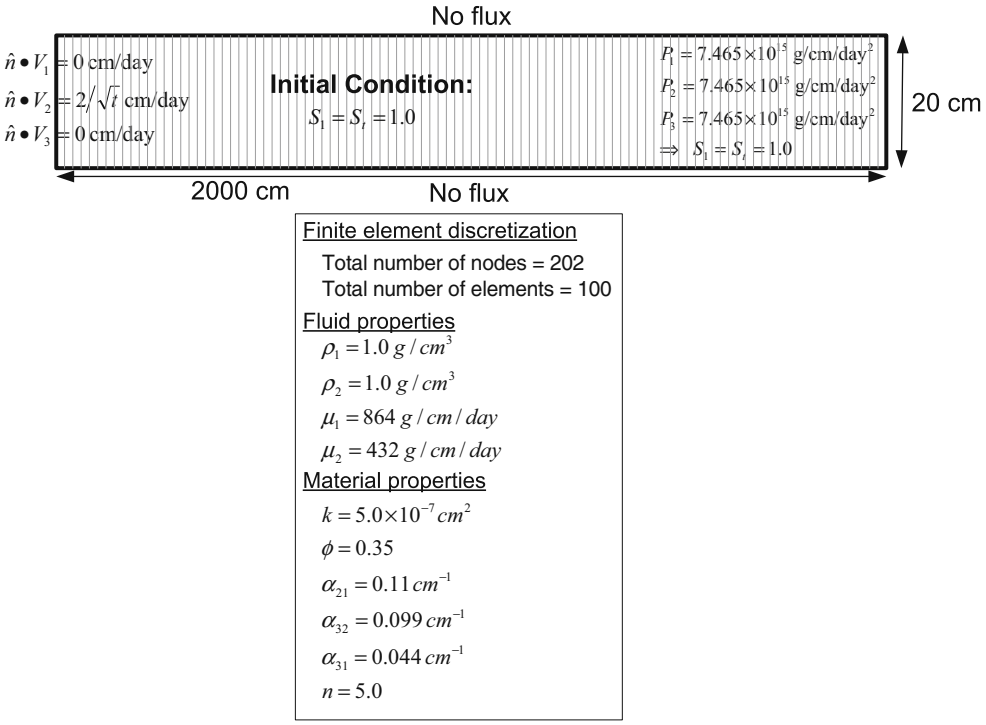

Fig. 3 Problem descriptions [13]: domain of interest, initial and boundary conditions, fluid properties, material properties, and finite element discretization

used here for model verification is described as follows: a one-dimensional, 2,000-cm long horizontal column of a porous media initially completely saturated by an incompressible wetting fluid, water. A non-wetting fluid is continuously injected at the inflow end of a column for $t > 0$ at a rate such that a constant water saturation $[S_1(0,t) = 0.84]$ is maintained at this boundary. To maintain constant saturation of wetting fluid at the inlet boundary by injection of non-wetting fluid, a parameter A in Eq. 81b can be determined analytically using the prescribed constant saturation [13]. The boundary and initial conditions for the displacement of a wetting phase by entry of a non-wetting phase are

$$n \bullet \mathbf{V}_1\,(0, t) = 0 \text{ for } t > 0, \tag{81a}$$

$$n \bullet \mathbf{V}_2\,(0, t) = At^{-1/2} \text{ for } t > 0, \tag{81b}$$

$$n \bullet \mathbf{V}_3\,(0, t) = 0 \text{ for } t > 0, \tag{81c}$$

$$P_1\,(2,000 \text{ cm}, t) = 7.465 \times 10^{15} \text{ g cm}^{-1} \text{ day}^{-2} \text{ for } t > 0, \tag{82a}$$

$$P_2\,(2,000 \text{ cm}, t) = 7.465 \times 10^{15} \text{ g cm}^{-1} \text{ day}^{-2} \text{ for } t > 0, \tag{82b}$$

$$P_3\,(2,000 \text{ cm}, t) = 7.465 \times 10^{15} \text{ g cm}^{-1} \text{ day}^{-2} \text{ for } t > 0, \tag{82c}$$

$$P_1\,(x, 0) = 7.465 \times 10^{15} \text{ g cm}^{-1} \text{ day}^{-2}, \tag{83a}$$

$$P_2\,(x, 0) = 7.465 \times 10^{15} \text{ g cm}^{-1} \text{ day}^{-2}, \tag{83b}$$

and

$$P_3\,(x, 0) = 7.465 \times 10^{15} \text{ g cm}^{-1} \text{ day}^{-2}, \tag{83c}$$

where the parameter is a constant. In this study, $A = 2$ cm/day$^{1/2}$ are chosen. In this paper, boundary condition at inlet is a type 1 in Table 2, and outflow boundary condition is a type 5 in Table 2. Similar as Section 4.1.2, three-phase pressures on the outflow boundary condition are determined so that both the water and total liquid saturations are 1.0. The air pressure is atmospheric pressure, and NAPL pressure is calculated from atmospheric air pressure using Eqs. 20 and 21, whereas water pressure is calculated from the calculated NAPL pressure using Eqs. 18 and 19. Thus, the pressures of water, NAPL, and air phases are given in Eqs. 82a, 82b, and 82c, respectively. This simulation illustrates that phase configuration is automatically changed from water-phase system to water/NAPL-phase system without any explicit assumption or criterion. For these conditions, the analytical solution is valid up to about 249 days, at which point the non-wetting front first almost reaches the end of the column. The input parameters used in this verification are indicated in Table 3. Figure 4 illustrates the excellent agree-

Table 3 Input parameters for comparison with analytical solutions

Parameter	Value	Units
Water-phase viscosity	μ_1=864.0	g cm^{-1} day^{-2}
NAPL-phase viscosity	μ_2=432.0	g cm^{-1} day^{-2}
Gas-phase viscosity	μ_3=15.812	g cm^{-1} day^{-2}
Van Genuchten fitting parameter	α_{21}=0.11	cm^{-1}
Van Genuchten fitting parameter	α_{32}=0.099	cm^{-1}
Van Genuchten fitting parameter	α_{31}=0.044	cm^{-1}
Porosity	$\phi = 0.35$	Dimensionless
Intrinsic permeability	$k = 5.0 \times 10^{-7}$	cm^2
Van Genuchten fitting parameter	$n = 5.0$	Dimensionless
Initial time-step size	1.0×10^{-5}	Day
Increment of time step	0.1	Dimensionless
Maximum time-step size	1.0	Day

ment between the numerical model and the analytical solution for the distribution of fluid saturations in the column at various times.

5 Results and discussions

To illustrate the treatment of general boundary conditions, seven example simulations are performed. The first example simulates water infiltration at constant water flux and constant atmospheric pressure, which is a combination of boundary condition types 2 and 5. The second example assumes NAPL infiltration under the constant total liquid saturation and simulates NAPL, water, and air saturation distributions in the simulation domain with boundary condition, which is a combination of types 5 and 8. In the third example, injection of incompressible air is applied in the three-phase system and simulates NAPL, water, and air saturation distribution with boundary condition, which is a combination of types 5 and 6. In the fourth example, initial conditions are assumed in steady state of water- and air-phase systems, and NAPL infiltration is applied at the top of boundary with boundary condition in the combination of types 3 and 5. In the fifth example, water infiltration with constant water pressure is applied at the top of boundary in the three-phase system with boundary condition in a combination of types 4 and 5. In the sixth example, NAPL infiltration is applied at the top boundary in a water-saturated porous media with boundary condition of type 7, and water and NAPL saturation distributions vary with time. In the seventh example, for the variable boundary condition and pumping well application, dense nonaqueous phase liquid (DNAPL) is spilled for an early period, and after some time, this DNAPL release suddenly stops, and a pumping well is simultaneously activated for remediation.

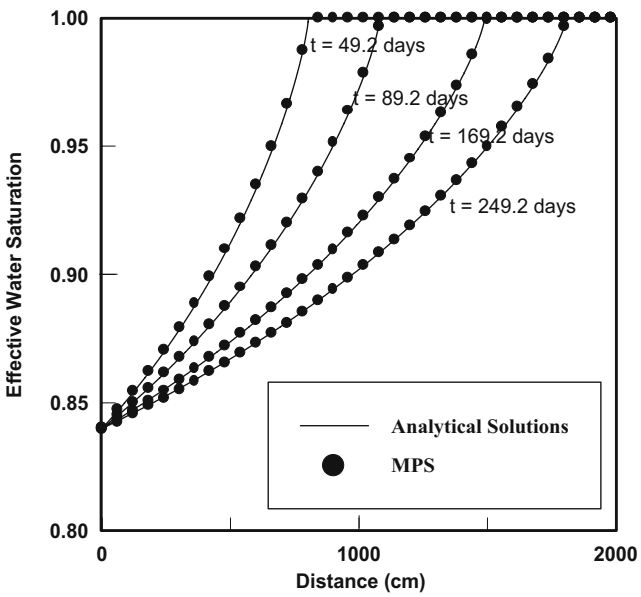

Fig. 4 Comparison of MPS solutions and exact solutions by McWhorter and Sunada [13] at various times

In addition, two more examples are simulated to illustrate the automatic adaptation of phase configuration change during the simulation period. Additionally, to show the capability of MPS model in two-dimensional area, the infiltration of a DNAPL in a fully water-saturated porous media is simulated to assess the effect of capillary media.

5.1 Water infiltration problem (boundary condition types 2 and 5)

Figure 5 depicts the conceptualization of this problem in terms of initial and boundary conditions, fluid properties, material properties, and finite element discretization. Water infiltration is applied at the top of a boundary at a water flux of a 10-cm/day, no flux of NAPL phase, and constant atmospheric pressure, which is type 2 in Table 2. The material and fluid properties are the same as the verification example in

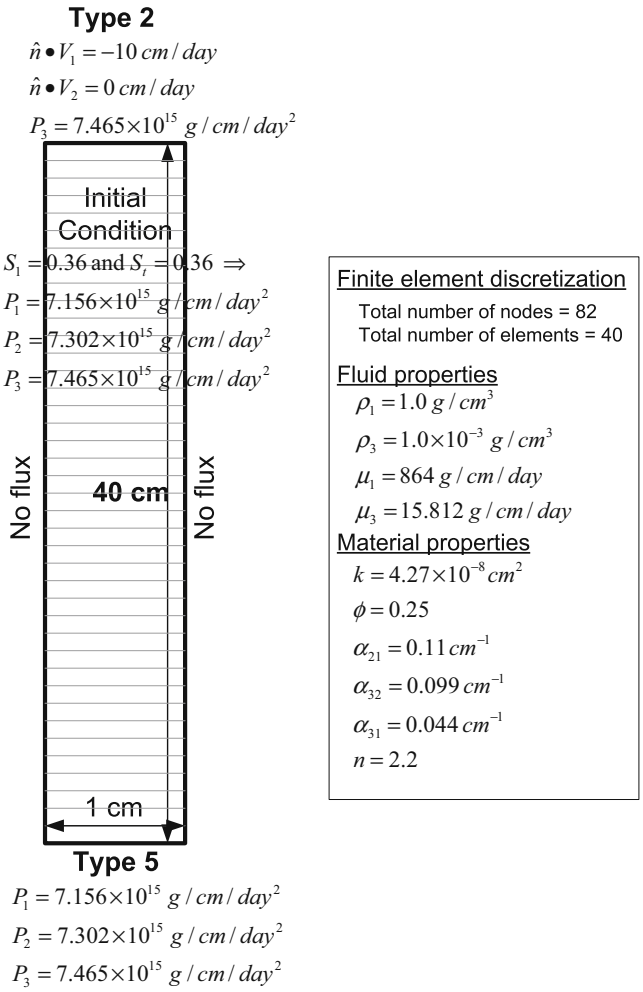

Fig. 5 Conceptual model for water infiltration: domain of interest, initial and boundary conditions, fluid properties, material properties, and finite element discretization

Section 4.1.1. In addition, grid discretization follows the example in Section 4.1.1. Initially, moisture content is uniformly equal to 0.36, and NAPL phase is absent throughout the simulation domain. To assign above initial conditions, initial condition type 1 in Table 1 is adopted, in which water pressure is equal to 7.156 × 10^{15} g cm^{-1} day^{-2}, NAPL pressure is a 7.302 × 10^{15} g cm^{-1} day^{-2}, and air pressure is equal to 7.465 × 10^{15} g cm^{-1} day^{-2}. These pressures of individual phases as initial conditions were calculated using capillary pressure–saturation relationships, Eqs. 18, 19, 20, and 21, assuming atmospheric air pressure. Because atmospheric air pressure is 7.465 × 10^{15} g cm^{-1} day^{-2} and total liquid saturation is 0.36, air–NAPL capillary head can be calculated from Eqs. 20 and 21. From the calculated air–NAPL capillary head, the NAPL pressure can be determined as 7.302 × 10^{15} g cm^{-1} day^{-2} using atmospheric air pressure. Similarly, using Eqs. 18 and 19 and the calculated NAPL pressure, the water pressure can be calculated as 7.156 × 10^{15} g cm^{-1} day^{-2} in order for the water saturation to be 0.36. Dirichlet boundary conditions are imposed at the bottom in the form of constant pressure of individual phases (boundary condition type 5 in Table 2). Air pressure is equal to 7.465 × 10^{15} g cm^{-1} day^{-2}, which is atmospheric pressure, NAPL pressure is 7.302 × 10^{15} g cm^{-1} day^{-2}, and water pressure is 7.156 × 10^{15} g cm^{-1} day^{-2}, all of which make water saturation and total liquid saturation equal to 0.36. In addition, as the

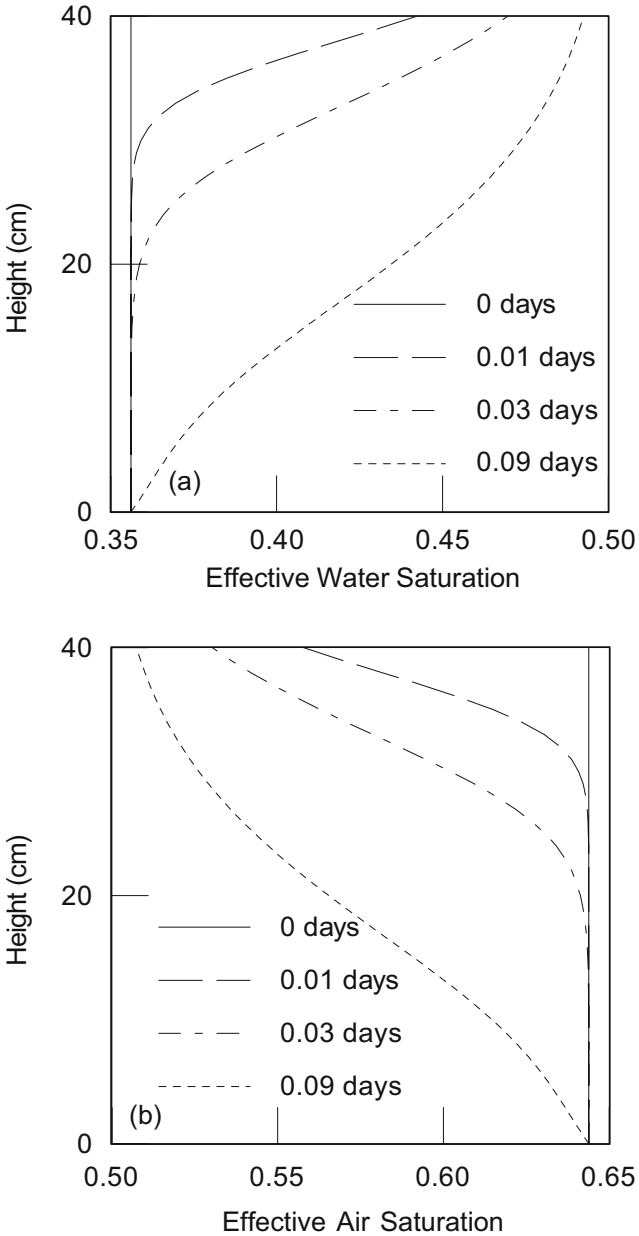

Fig. 6 Distributions of **a** water saturation and **b** air saturation at various times for problem 5.1

initial condition, these specified pressures of individual phases could be determined using capillary pressure–saturation relationships. The left and right sides are no flux conditions for three phases. The water saturation distributions and air saturation distributions at various times are shown in Fig. 6. As shown in Fig. 6, as the water infiltrates into the soil column, air is displaced out from the top of soil.

5.2 NAPL infiltration with constant total liquid saturation (types 5 and 8)

Figure 7 depicts the conceptualization of this problem in terms of initial and boundary conditions, fluid and material properties, and finite element discretization. NAPL infiltration is applied with constant total liquid saturation of St = 0.53 and zero water flux on the top of the soil column (boundary condition type 8 in Table 2). In order that constant total liquid saturation of 0.53 is applied, NAPL phase pressure equal to 7.360×10^{15} g cm^{-1} day^{-2} and air-phase pressure equal to 7.465×10^{15} g cm^{-1} day^{-2} are specified on the top boundary. Specified pressures of NAPL and air for boundary condition type 8 can be calculated using the capillary pressure–saturation relationships, Eqs. 20 and 21, with assumption of atmospheric air pressure in order that the total liquid saturation is 0.53. On the bottom, the constant pressures of all three individual phases are maintained to make water, NAPL, and air saturations equal to 0.36, 0.00, and 0.64, respectively. Initially, it is assumed that water moisture content has the 0.36 saturation, NAPL has the zero saturation, and air has the saturation of 0.64. To assign these initial conditions,

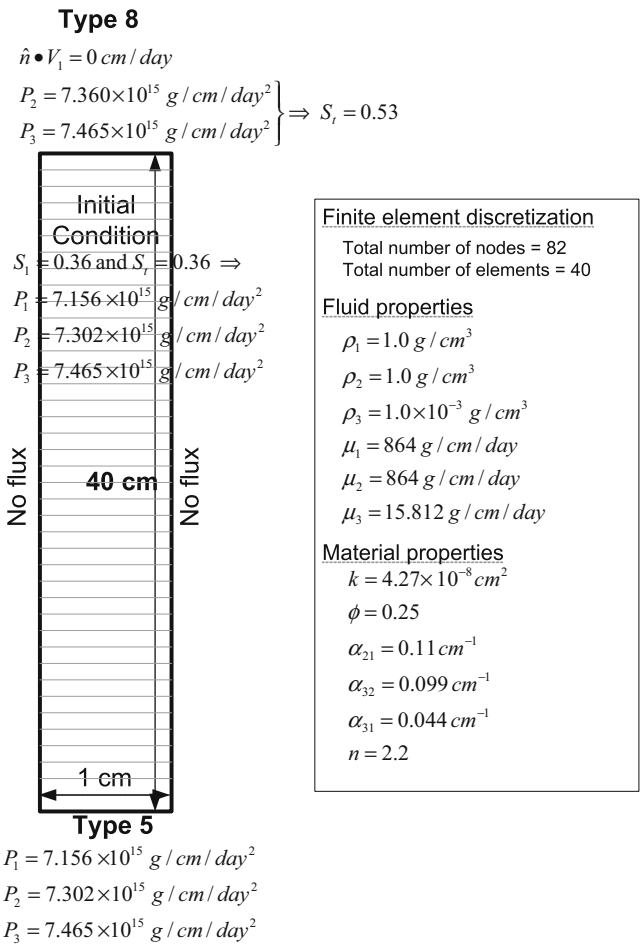

Fig. 7 Conceptual model for NAPL infiltration: domain of interest, initial and boundary conditions, fluid properties, material properties, and finite element discretization

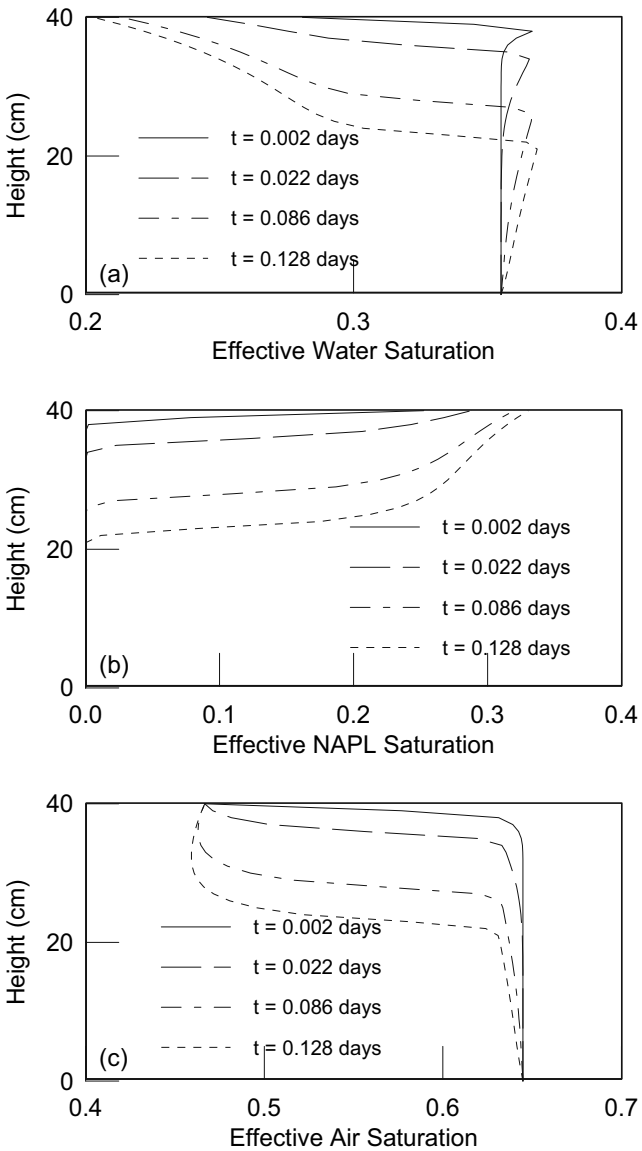

Fig. 8 Distributions of **a** water saturation, **b** NAPL saturation, and **c** air saturation at various times for problem 5.2

initial condition type 1 in Table 1 is employed, in which water pressure is equal to 7.156×10^{15} g cm^{-1} day^{-2}, NAPL pressure is a 7.302×10^{15} g cm^{-1} day^{-2}, and air pressure is equal to 7.465×10^{15} g cm^{-1} day^{-2}. The left and right sides have no flux conditions for three phases. Figure 8 shows that water is displaced by infiltrating NAPL forming the small pool at the front of NAPL infiltration and also air is displaced out from the top. As water is not allowed to escape (zero flux boundary condition on the top), an overshooting in water saturation is created due to the infiltrating liquid. Note that sum of water and NAPL saturations are always 0.53 on the top of soil column and also air saturation always maintains at 0.47 on the top boundary because constant total liquid saturation is used for the boundary condition. Furthermore, this simulation shows automatic phase configuration change from two-phase system of water–air to three-phase system of water–NAPL–air in the simulation domain without any explicit assumption or criterion on the phase appearance and disappearance.

5.3 Injection of incompressible air into three-phase system (types 5 and 6)

This problem, in terms of initial and boundary conditions and fluid and material properties, is depicted in Fig. 9. The finite element discretization for numerical simulations is also shown. Injection of incompressible air into three-phase system is performed at a rate of 10 cm/day on the top boundary, and Dirichlet boundary conditions are imposed at the top in the form of constant water pressure and NAPL pressure, which are 7.156×1015 and 7.392×10^{15} g cm^{-1} day^{-2}, respectively. On the top boundary, constant water pressure

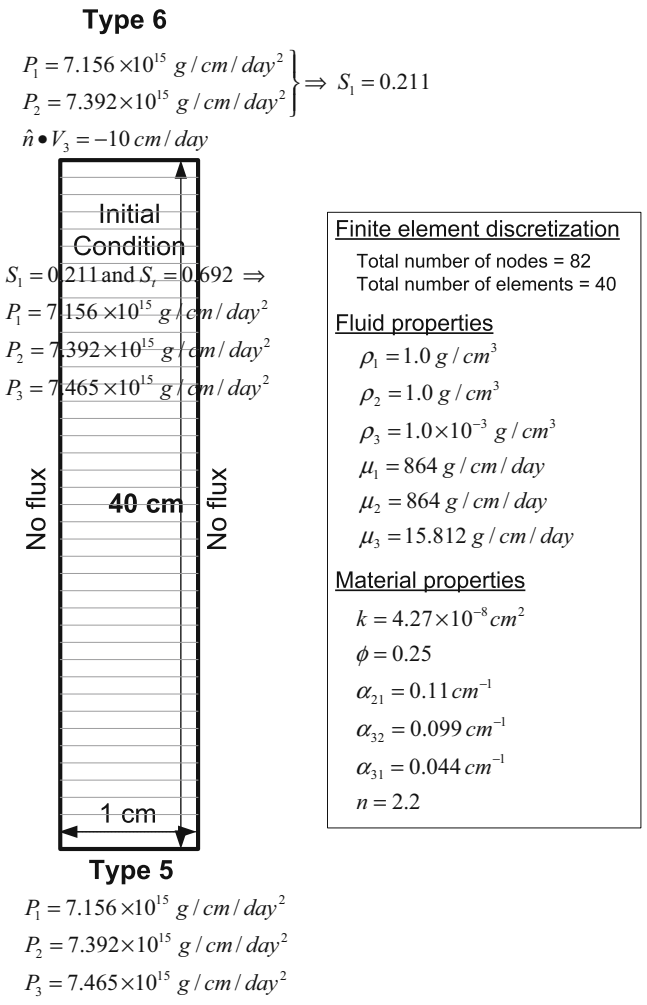

Fig. 9 Conceptual model for injection of incompressible air into a three-phase system: domain of interest, initial and boundary conditions, fluid properties, material properties, and finite element discretization

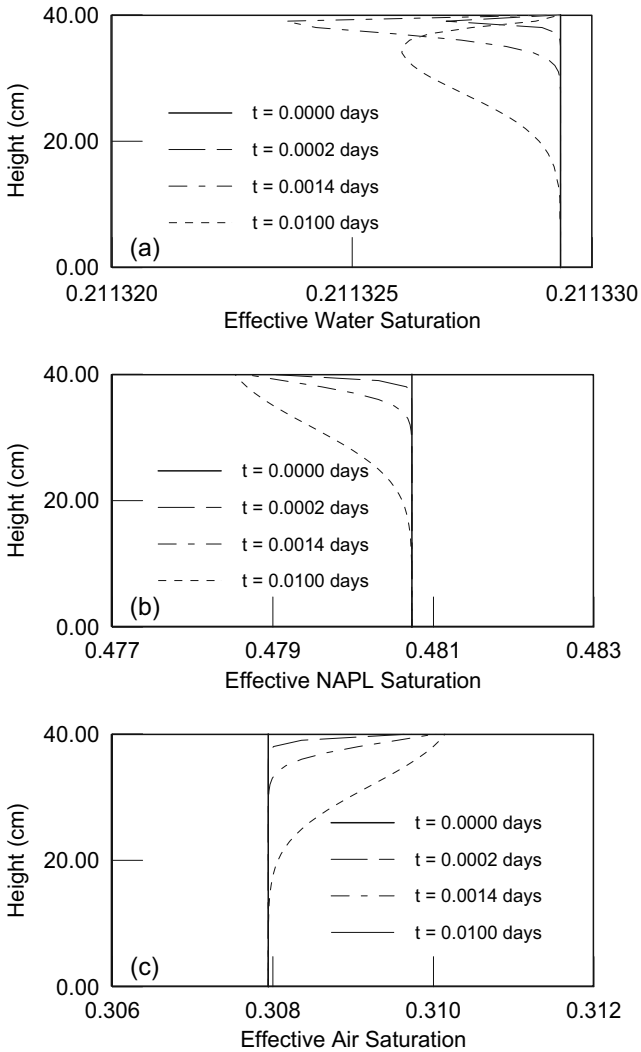

Fig. 10 Distributions of **a** water saturation, **b** NAPL saturation, and **c** air saturation at various times for problem 5.3

and NAPL pressure make the water saturation equal to 0.211329. Boundary condition at the top corresponds to type 6 in Table 2. On the base of the soil column, Dirichlet-type boundary conditions are specified for all three-phase pressures, which correspond to type 5 in Table 2. In this study, water pressure is specified as 7.156×10^{15} g cm^{-1} day^{-2}, NAPL pressure is specified as 7.392×10^{15} g cm^{-1} day^{-2}, and air pressure is specified as 7.465×10^{15} g cm^{-1} day^{-2} so that water saturation, NAPL saturation, and air saturation are 0.211, 0.481, and 0.308, respectively. For the initial condition, initial condition type 1 in Table 1 is employed so that water saturation, NAPL saturation, and air saturation are 0.211, 0.481, and 0.308, respectively. In the initial condition type 1, water pressure, NAPL pressure, and air pressure are 7.156 × 1015, 7.392 × 1015, and 7.465 × 10^{15} g cm^{-1} day^{-2}, respectively. As shown in Fig. 10, air displaces water and NAPL, as the air goes into the three-phase system. Notice that water has constant saturation over the time on the top, but the NAPL has decreasing saturation with time. This difference between water and NAPL comes from the fact that water has constant saturation boundary condition on the top boundary.

5.4 NAPL infiltration into the steady-state two-phase system of water–air under the constant NAPL pressure (types 3 and 5)

This problem is conceptually depicted in Fig. 11. Initial water pressure is assumed to follow a static pressure distribution in the vertical soil column. This means that gravity force and capillary force are at equilibrium of each other. Therefore, initially, water content is in-

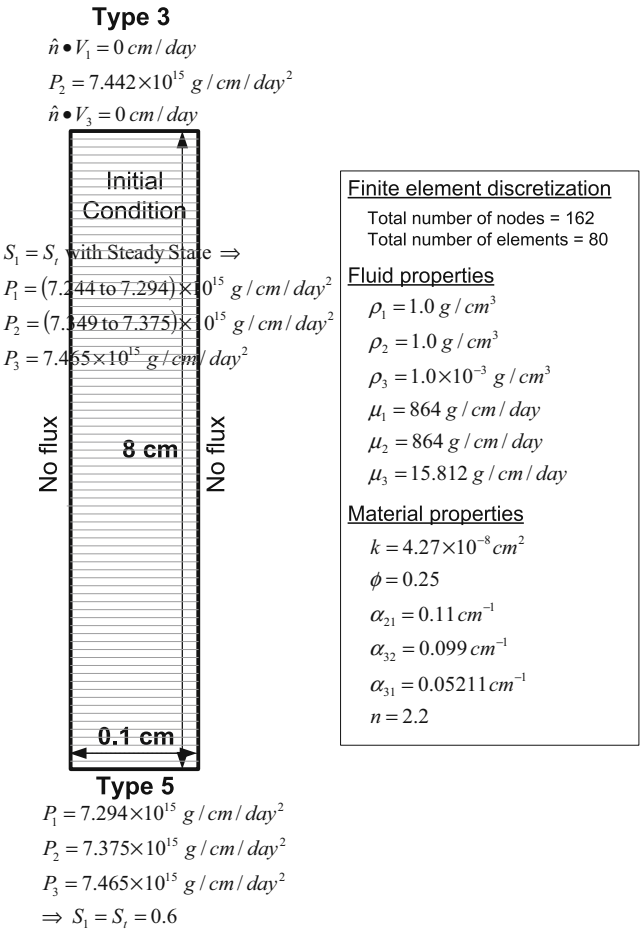

Fig. 11 Conceptual model for NAPL infiltration via constant NAPL pressures at the boundaries: domain of interest, initial and boundary conditions, fluid properties, material properties, and finite element discretization

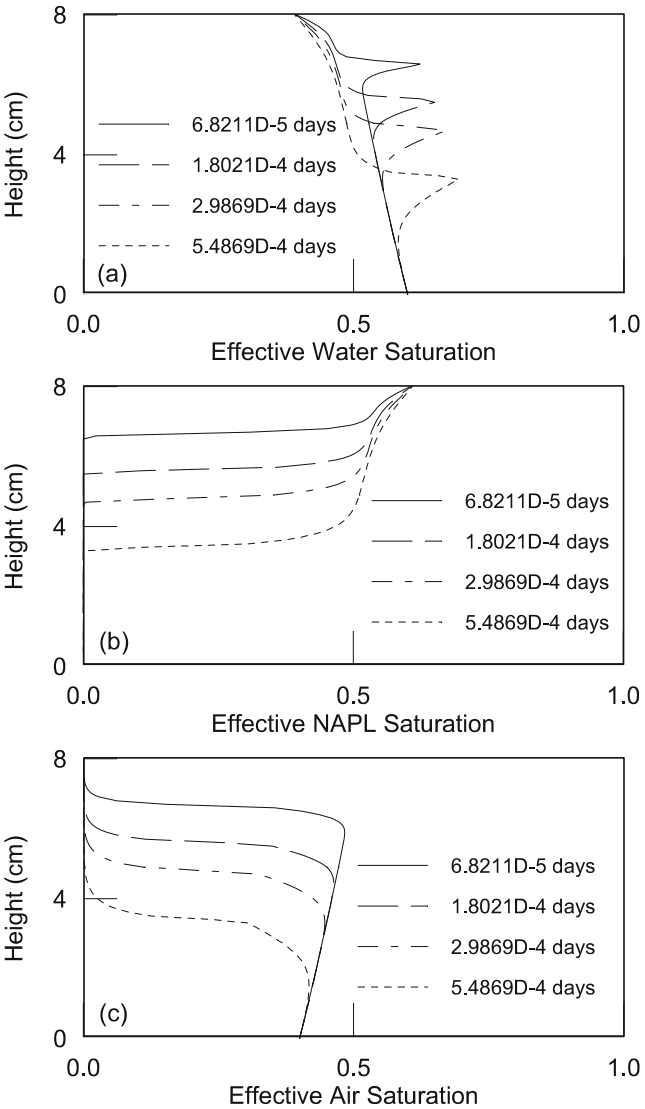

Fig. 12 Distributions of **a** water saturation, **b** NAPL saturation, and **c** air saturation at various times for problem 5.4

creased from top to bottom. At the top of the boundary, boundary condition of type 3 is applied, in which water and air flux is zero and NAPL-phase pressure is 7.442×10^{15} g cm^{-1} day^{-2}. NAPL is infiltrated into the two-phase system of water–air in steady-state condition under the constant NAPL-phase pressure. In addition, boundary condition of type 5 is specified at the bottom boundary, in which water pressure is 7.294×10^{15} g cm^{-1} day^{-2}, NAPL pressure is 7.375×10^{15} g cm^{-1} day^{-2}, and air pressure is 7.465×10^{15} g cm^{-1} day^{-2} so that water saturation is 0.6, NAPL saturation is 0.00, and air saturation is 0.4. As shown in Fig. 12, the NAPL saturation increases from toward the top, air saturation decreases from the top, whereas water forms small ripples at the front of the NAPL phase. The feature is that wetting phase water is not much affected by NAPL, whereas the non-wetting phase, air, is much more affected. Furthermore, this simulation result shows that automatic phase configuration is changed from the two-phase system of water–air to the three-phase system of water–NAPL–air in the simulation domain without any explicit assumption or criterion about the phase appearance and disappearance.

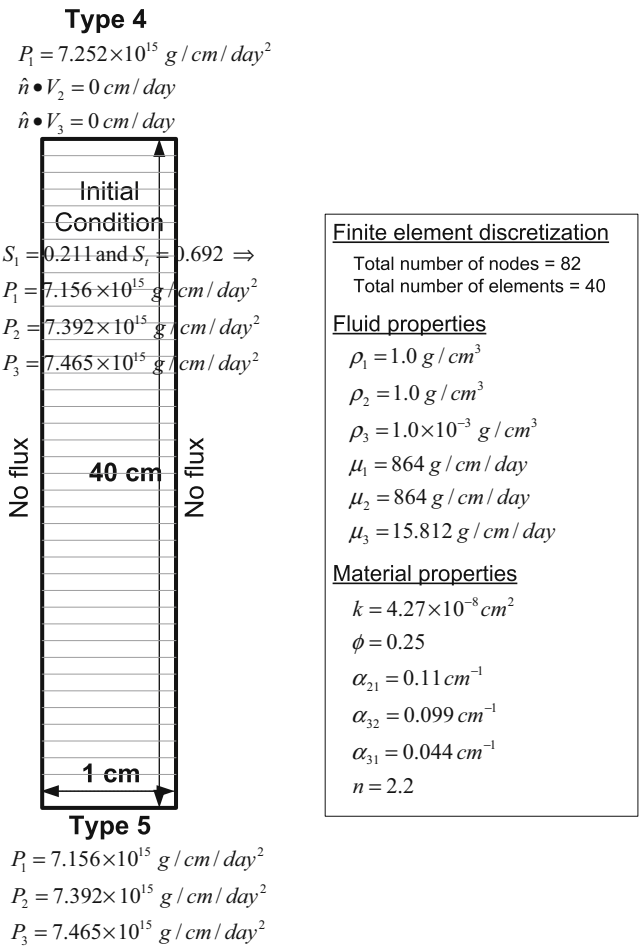

Fig. 13 Conceptual model for water infiltration into a three-phase system: domain of interest, initial and boundary conditions, fluid properties, material properties, and finite element discretization

5.5 Water infiltration in a three-phase system with constant water pressure (types 4 and 5)

This problem is conceptually depicted in Fig. 13. At the top boundary, water infiltration is applied with the boundary condition of type 4, in which water pressure is 7.252×10^{15} g cm^{-1} day^{-2} and NAPL and air fluxes are zero. Initially, a three-phase system is assumed so that water saturation is 0.211, NAPL saturation is 0.481, and air saturation is 0.308. To assign these initial conditions, water pressure is specified as 7.156×10^{15} g cm^{-1}

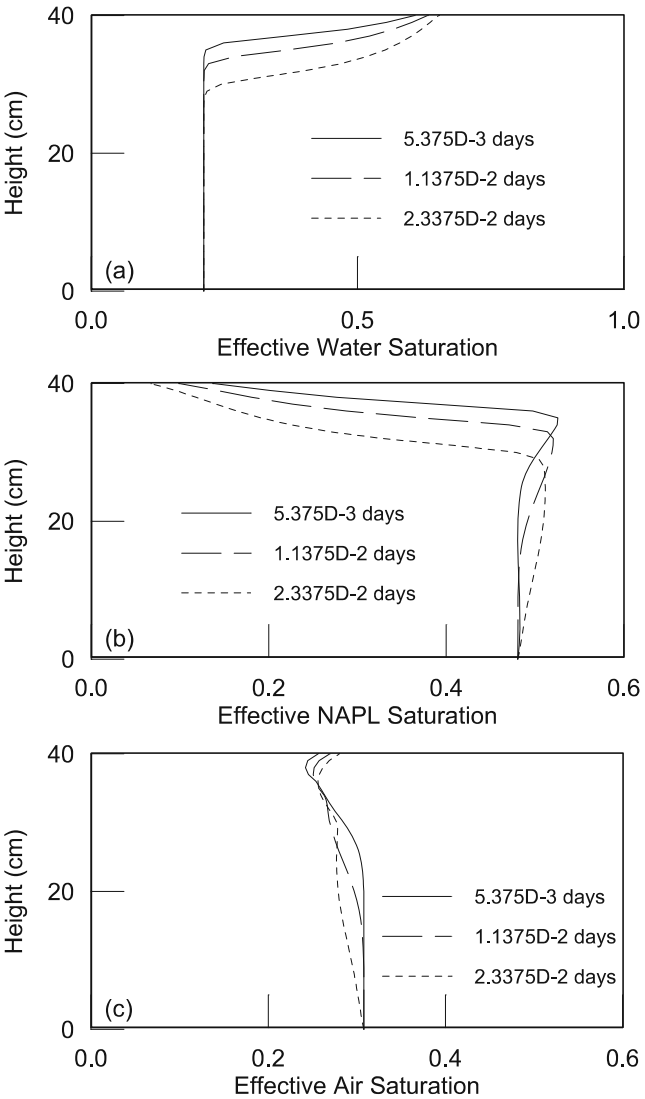

Fig. 14 Distributions of **a** water saturation, **b** NAPL saturation, and **c** air saturation at various times for problem 5.5

day^{-2}, NAPL pressure is assumed as 7.392 $\times$ 10^{15} g cm^{-1} day^{-2}, and air pressure is assumed as 7.465 $\times$ 10^{15} g cm^{-1} day^{-2}. In addition, the bottom boundary is specified with the boundary condition of type 5 so that water saturation, NAPL saturation, and air saturation are maintained at 0.211, 0.481, and 0.308, respectively. Figure 14 shows that water displaces NAPL and air from the top and NAPL saturation and air saturation are decreased, whereas water saturation increases toward the top.

5.6 NAPL infiltration into fully water-saturated porous media with NAPL flux boundary condition (Types 7 and 5)

This problem is conceptually described in Fig. 15. NAPL infiltration is applied at the top boundary of fully water-saturated porous media with type 7 boundary condition, in which both water and air pressures are specified at 7.465 $\times$ 10^{15} g cm^{-1} day^{-2} and NAPL flux is given at a rate of 100 cm/day. Furthermore, at the bottom boundary, the boundary condition of type 5 is made such that water saturation is always maintained at 1. Figure 16 shows that NAPL displaces water, so NAPL saturations increase with time toward the top of the boundary, whereas water saturations decrease. As with the verification example in Section 4.2, the phase system is automatically changed from water-saturated system to water–NAPL system without any explicit

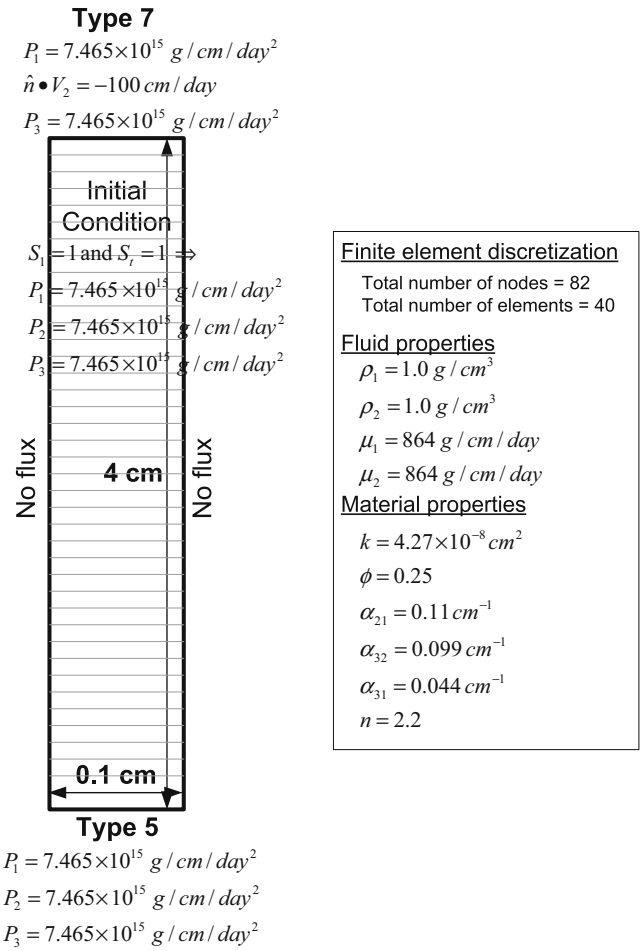

Fig. 15 Conceptual model for NAPL infiltration into water-saturated porous media: domain of interest, initial and boundary conditions, fluid properties, material properties, and finite element discretization

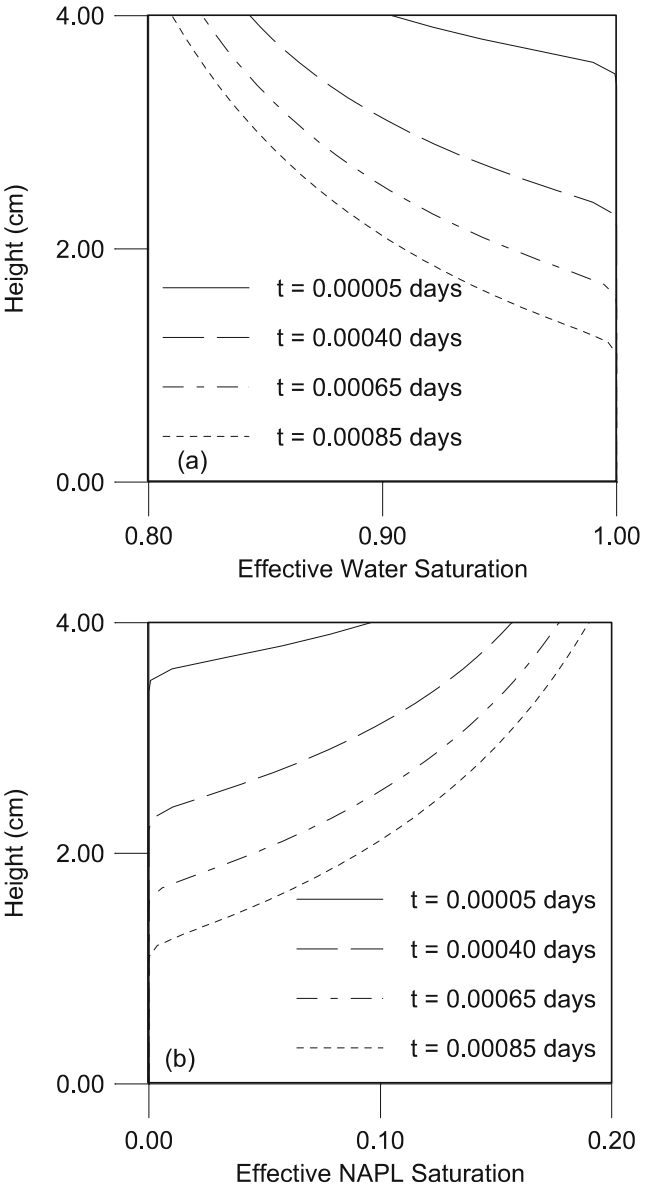

Fig. 16 Distributions of **a** water saturation and **b** NAPL saturation at various times for problem 5.6

assumption or criteria about phase configuration change in the domain. As type 7 is a highly nonlinear character boundary condition, outer nonlinear boundary iteration number almost ranges from 4 to 10, which is the most among all examples presented in this paper.

5.7 DNAPL spill and cleanup with variable boundary conditions

This problem is portrayed in Fig. 17. The DNAPL is infiltrated from a spill area for 3.226 days under the hydraulic gradient in which the ambient water flow direction goes from left to right with a rate of 40 cm/day. After 3.226 days, the infiltration of DNAPL is suddenly stopped, and cleanup is started using pumping wells with a pumping rate 1,000 cm^3 day-1 for the remainder of the simulation time. It is assumed that the DNAPL is infiltrated at a rate of 10 cm/day into the initially water-saturated system with a variable boundary condition. Total simulation time is 5.4419 days.

The intrinsic permeability of an aquifer is 1.0×10^{-8} cm^2, and porosity is 0.38. Water density is 1.0 g/cm^3, and DNAPL density is 1.4 g/cm^3. Water viscosity is 864.0 g cm^{-1} day^{-1}, and DNAPL viscosity is 690.0 g cm^{-1} day^{-1}. Van Genuchten parameters are set to $\alpha_{21} = 0.009$, n = 2.8. To simulate this example, the domain of interest is discretized with a total of 200 nodes and 171 elements. The boundary conditions are shown in Fig. 17. The left boundary condition is prescribed with boundary condition of

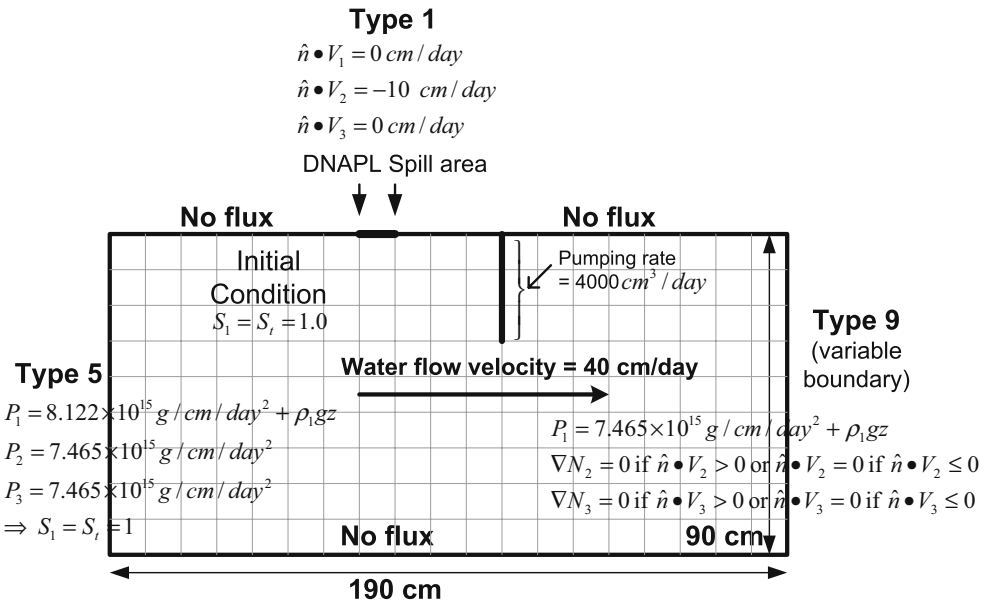

Fig. 17 DNAPL spill and cleanup simulated with boundary-type switching (variable boundary condition): domain of interest, initial and boundary conditions, fluid properties, material properties, and finite element discretization. ΔN2 and ΔN3 are capillary gradient for NAPL and air phase, respectively

type 5, and right boundary condition is specified with boundary condition of type 9. On the left boundary, the hydrostatic pressure of the water phase is assumed. The right boundary is a water medium interface, on which the water pressure is prescribed, but neither the NAPL flux nor the NAPL pressure is known a priori; thus, the variable-boundary condition is used. In the DNAPL spilled area of Fig. 17, boundary condition of type 1 is applied so that only the DNAPL phase is infiltrated with a rate of 10 cm/day. The remainder of the top boundary is applied with no-flow boundary condition. Similarly, no-flow boundary conditions are applied to the bottom side as shown in Fig. 17. The initial condition is set as follows: water and total liquid saturations are both 1, respectively. This problem is solved with MPS. The simulation results are shown in Figs. 18, 19, and 20. Figure 18 shows streamlines of water at various times. Initially water streamline is horizontal, as direction of hydraulic gradient is from left to right and also streamline is not much affected by DNAPL infiltration as shown in Fig. 18b. However, at the start of the pumping period, streamline is greatly

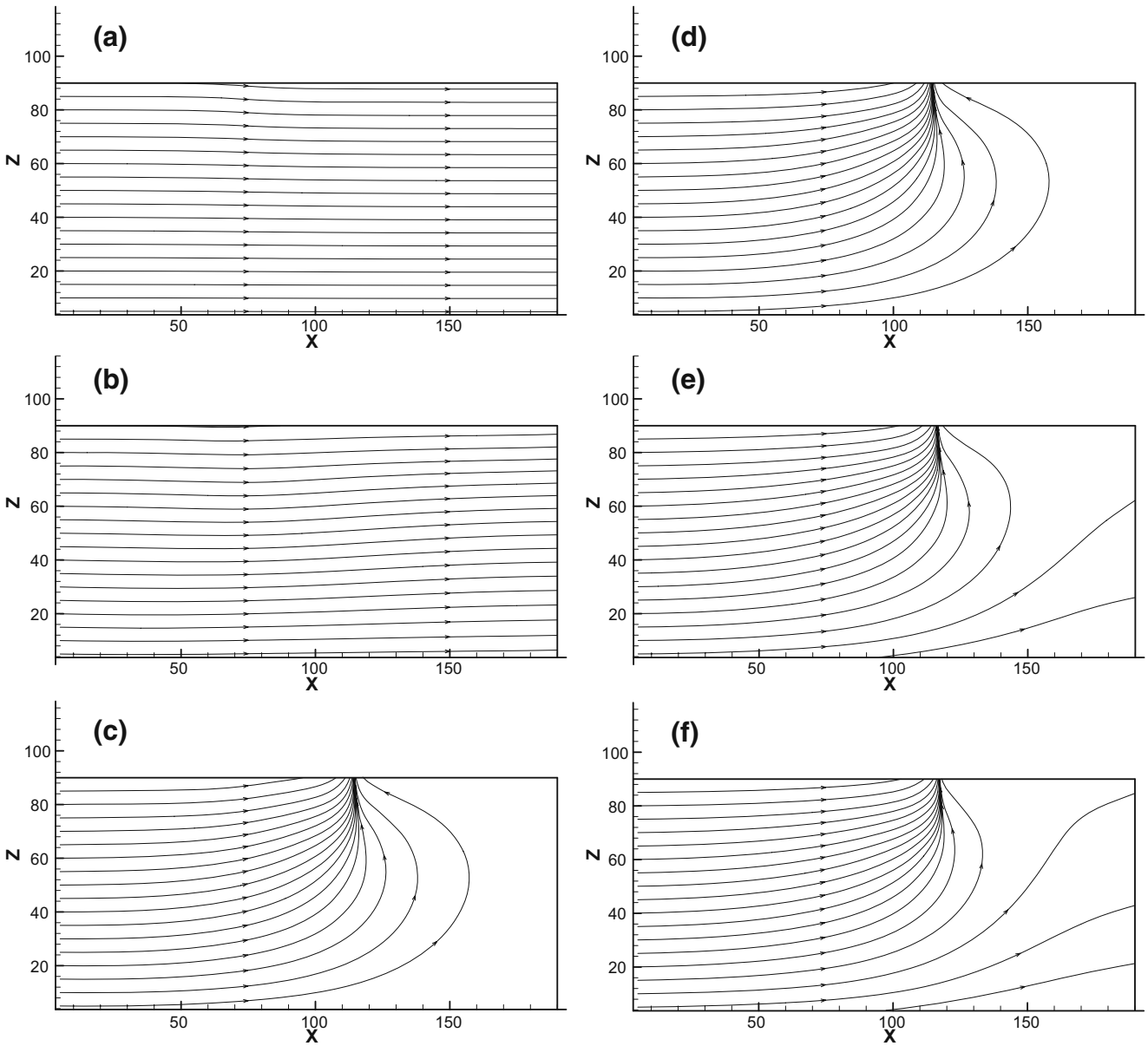

Fig. 18 Streamlines of water phase at various times for problem 5.7: **a** 1.0×10^{-5} days and **b** 3.226 days, **c** 3.2261 days, **d** 3.2509 days, **e** 3.8867 days, and **f** 5.4419 days

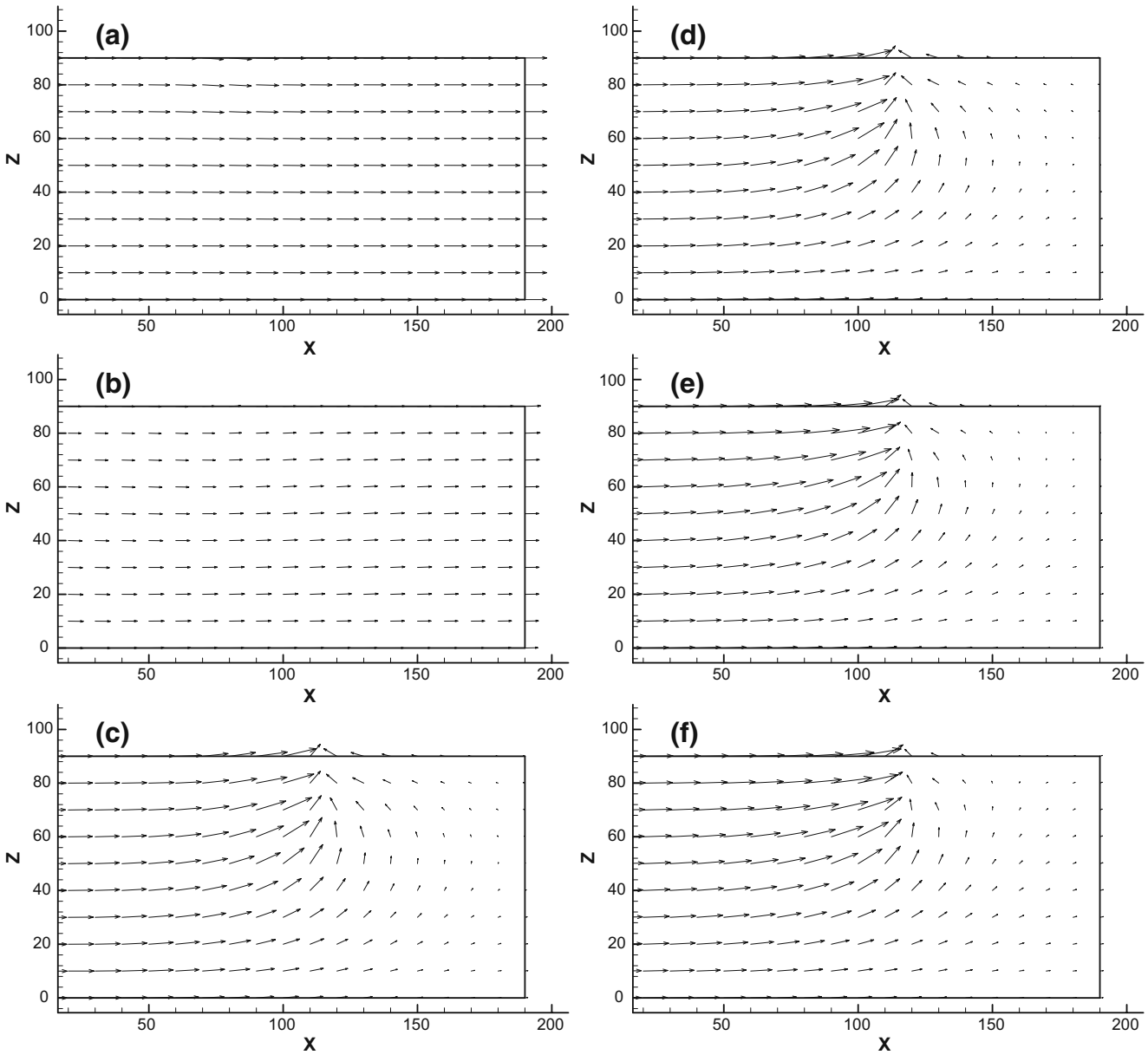

Fig. 19 Velocity distribution of water phase at various times for problem 5.7: **a** 1.0 $\times 10^{-5}$ days and **b** 3.226 days, **c** 3.2261 days, **d** 3.2509 days, **e** 3.8867 days, and **f** 5.4419 days

changed so that the tracking path of most of the water goes toward pumping well as shown in Fig. 18c. As the time increases, as shown in Fig. 18d–f, streamlines of the water phase at the downward direction of the well is much more evolved in a direction parallel to the ambient water direction, as DNAPL has been depleted due to downward movement by gravity force and water can easily pass through right lower part of the simulation domain against DNAPL. Figure 19 shows velocity distributions of water phase at various times. Similarly, as streamlines of the water phase, initial water velocity is directed from left to right (Fig. 19a), but as DNAPL infiltrates, although the direction of water-phase velocity is little changed, the magnitude of water-phase velocity is decreased, as DNAPL retards water flow (Fig. 19b). At the start of pumping, the direction of water velocity is greatly altered, as most of the water has undergone attraction toward the pumping well as shown in Fig. 19c. During pumping (Fig. 19d–f), the steady-state solution is reached quickly because the storage effect of the medium and liquids is not included. Figure 20 shows distributions of DNAPL velocity and distributions of DNAPL saturation. In the initial DNAPL, the velocity is zero in the whole domain,

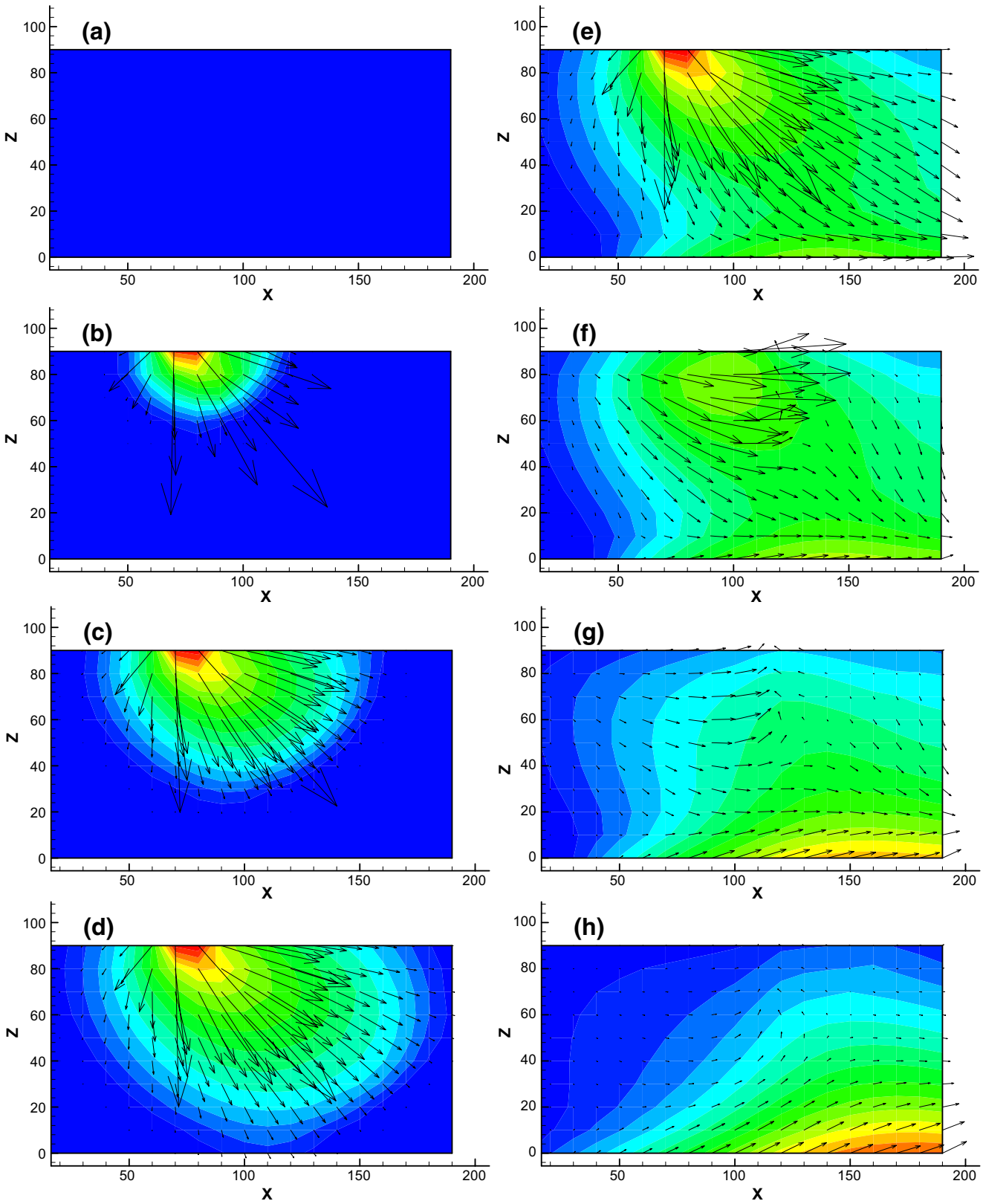

Fig. 20 Distributions of DNAPL velocity and DNAPL saturation plots at various times for problem 5.7: **a** 1.0×10^{-5} days and **b** 3.3604×10^{-1} days, **c** 1.136 days, **d** 1.936 days, **e** 3.226 days, **f** 3.2936 days, **g** 3.7867 days, and **h** 5.4419 days

as DNAPL is initially absent in the whole domain as shown in Fig. 20a. As DNAPL is infiltrated, the DNAPL saturation is increased at the neighborhood of a source area; thus, the velocity of DNAPL is increased as shown in Fig. 20b. Note that, where the DNAPL is absent, the DNAPL velocity is zero. As DNAPL continuously infiltrates, more area of simulation domain has nonzero DNAPL velocity as shown in Fig. 20c, d. As the variable boundary condition plays a role on flow going out via the boundary, DNAPL passes through the right boundary side. Figure 20e shows the distribution of the DNAPL velocity when DNAPL reaches right boundary side. When the DNAPL infiltration is stopped and the operation of the pumping well begins, the DNAPL velocity in the vicinity of well is greatly changed, as DNAPL goes toward pumping well as shown in Fig. 20f. As the time increases, the DNAPL saturation is decreased in the vicinity of the pumping well; thus, the magnitude of DNAPL velocity is greatly decreased (Fig. 20g, h).

5.8 Water movement in the capillary fringe (from a water–air system to a water-only system)

This problem is depicted in Fig. 21. Water movement in the capillary fringe in a column is simulated using the Dirichlet boundary condition. The column has a length of 40 cm and width of 1 cm. The 40-cm column is discretized into uniform nodal spacing of 1 cm in the vertical direction. Initially, the moisture content is uniform, $S_1 = 0.69$, throughout the column ($S_2 = 0$ and $_3 = 0.31$, initial condition Type 8 in Table 1). Dirichlet boundary conditions are imposed at the top in the form of constant pressure of individual phases (boundary condition type 5 in Table 2). Air pressure is equal to 7.465×10^{15} g cm^{-1} day^{-2}. NAPL pressure is 7.258×10^{15} g cm^{-1} day^{-2}, and water pressure is 7.072×10^{15} g cm^{-1} day^{-2}, which make water saturation and total liquid saturation equal to 0.28. The base of the column is maintained at constant pressures of individual phases throughout the simulation, which are all same pressure 7.465×10^{15} g cm^{-1} day^{-2} (boundary condition type 5 in Table 2). The three pressures make water saturation = total liquid saturation equal to 1. The left and right sides are no flux conditions for three phases. Simulation information is summarized in Table 4. The water saturation distributions at various times are shown in Fig. 22 using various solvers. Figure 22 shows upward movement of water with time due to effect of capillary pressure at the base. Finally, steady state is attained after about 1.0 day. The simulation shows automatic phase configuration change from a two-phase system of water–air to a water-only saturated system over time in Fig. 22. Furthermore, Fig. 22 indicates that different solvers produce almost identical solutions: bi-conjugate-gradient-stabilized solver (Bi-CGSTAB) method [18], Modified incomplete Cholesky preconditioned conjugate-gradient solver (MICPCG), direct Gaussian elimination method, and pointwise iterative solution strategies (PISS). The discussion on convergent rate is beyond the scope of this paper, although we noted that Bi-GGSTAB is fastest for this particular example.

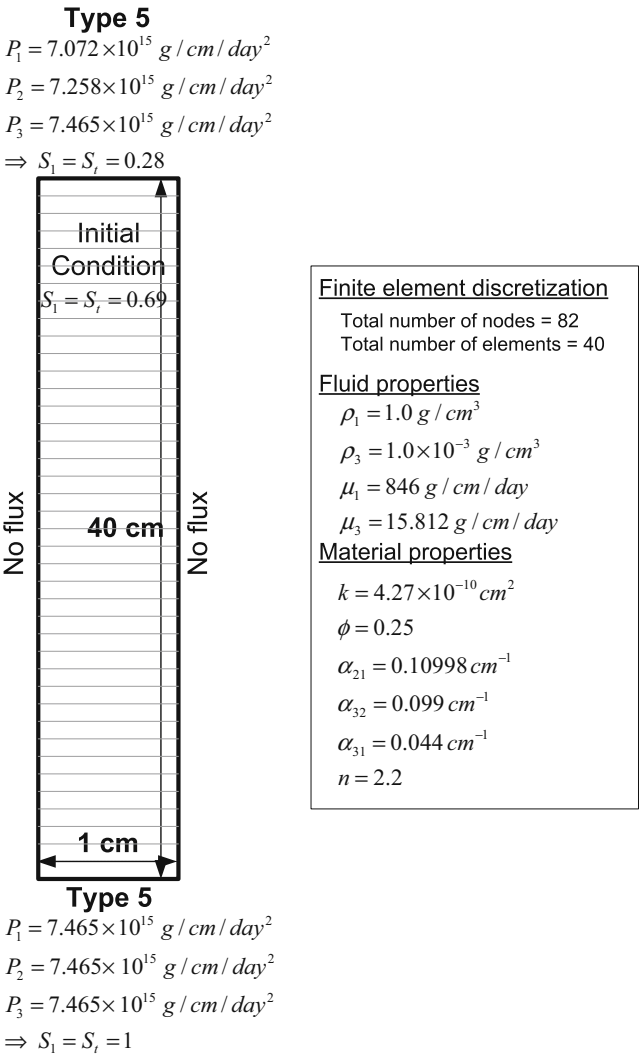

Fig. 21 Water movement due to capillary fringe rises that transform an initially water–air system to a water-only system: domain of interest, initial and boundary conditions, fluid properties, material properties, and finite element discretization

Table 4 Input parameters for simulation of water movement in the capillary fringe

Parameter	Value	Units
Intrinsic permeability	$k = 4.27 \times 10^{-10}$	cm^2
Water-phase density	$\rho_1 = 1.0$	g/cm^3
NAPL-phase density	$\rho_2 = 1.0$	g/cm^3
Gas-phase density	$\rho_3 = 1.0 \times 10^{-3}$	g/cm^3
Water-phase viscosity	$\mu_1 = 846.0$	$g\ cm^{-1}\ day^{-2}$
NAPL-phase viscosity	$\mu_2 = 846.0$	$g\ cm^{-1}\ day^{-2}$
Gas-phase viscosity	$\mu_3 = 15.812$	$g\ cm^{-1}\ day^{-2}$
Van Genuchten fitting parameter	$\alpha_{21} = 0.10998$	cm^{-1}
Van Genuchten fitting parameter	$\alpha_{32} = 0.099$	cm^{-1}
Van Genuchten fitting parameter	$\alpha_{31} = 0.044$	cm^{-1}
Van Genuchten fitting parameter	$n = 2.2$	Dimensionless
Porosity	$\phi = 0.25$	Dimensionless
Initial time-step size	5.0×10^{-6}	Day
Increment of time step	0.01	Dimensionless
Maximum time-step size	1.0×10^{-3}	Day

5.9 NAPL infiltration by flux boundary condition (from a water–air system to a water–NAPL–air system)

This problem is conceptually depicted in Fig. 23. Usually, boundary conditions are the Dirichlet type, which is not practical for real problems because it is impossible to know the pressure of infiltrating phases over time. However, in this example, flux boundary conditions are assigned at the top of the soil column. NAPL phase flux at the top is equal to 10.0 cm/day, but air- and

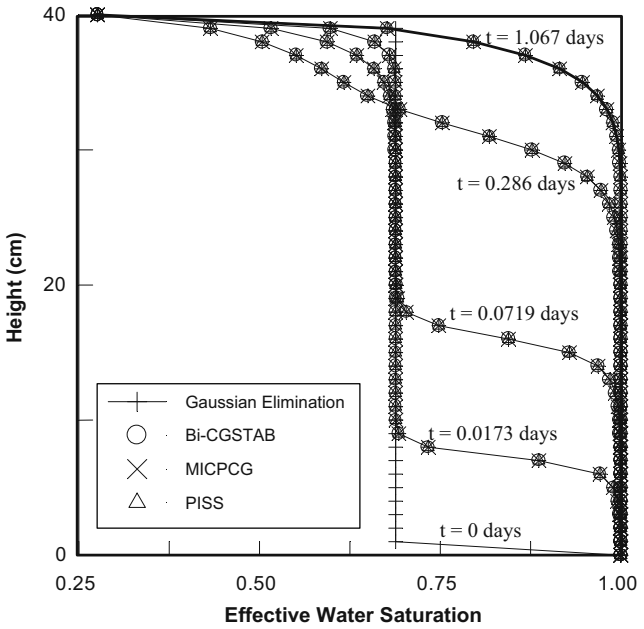

Fig. 22 Comparison of numerical solutions of various solvers at various times for problem 5.8: Bi-CGSTAB, MICPCG, PISS, and direct Gaussian elimination method

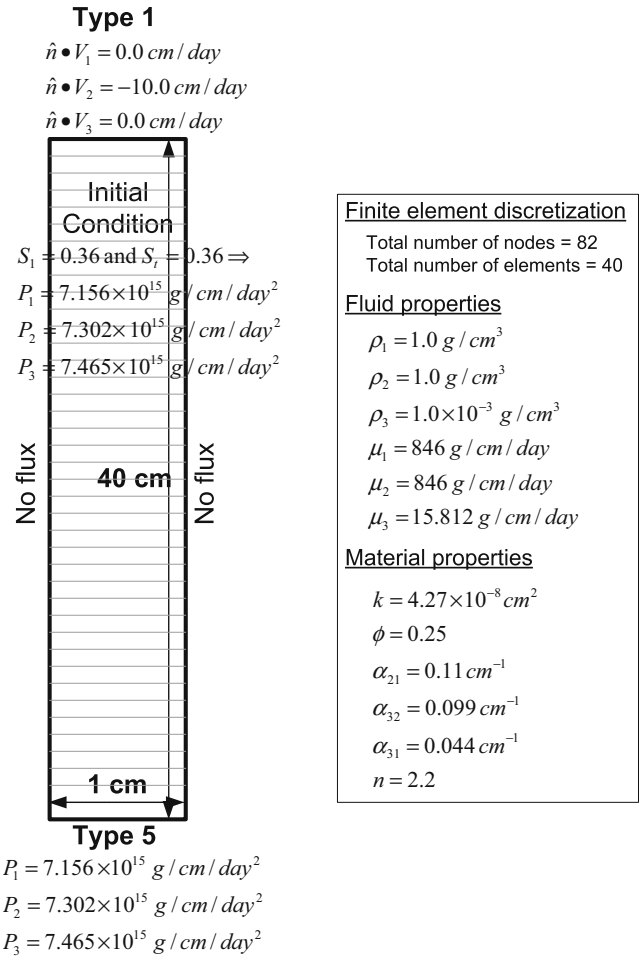

Fig. 23 NAPL infiltration via boundary fluxes, which transform an initially water–air system to a water–NAPL–air system: domain of interest, initial and boundary conditions, fluid properties, material properties, and finite element discretization

Table 5 Input parameters for simulation of NAPL infiltration on the top

Parameter	Value	Units
Intrinsic permeability	$k = 4.27 \times 10^{-8}$	cm^2
Water-phase density	$\rho_1 = 1.0$	g/cm^3
NAPL-phase density	$\rho_2 = 1.0$	g/cm^3
Gas-phase density	$\rho_3 = 1.0 \times 10^{-3}$	g/cm^3
Water-phase viscosity	$\mu_1 = 846.0$	$g\ cm^{-1}\ day^{-2}$
NAPL-phase viscosity	$\mu_2 = 846.0$	$g\ cm^{-1}\ day^{-2}$
Gas-phase viscosity	$\mu_3 = 15.812$	$g\ cm^{-1}\ day^{-2}$
Van Genuchten fitting parameter	$\alpha_{21} = 0.11$	cm^{-1}
Van Genuchten fitting parameter	$\alpha_{32} = 0.099$	cm^{-1}
Van Genuchten fitting parameter	$\alpha_{31} = 0.044$	cm^{-1}
Van Genuchten fitting parameter	$n = 2.2$	Dimensionless
Porosity	$\phi = 0.25$	Dimensionless
Initial time-step size	5.0×10^{-5}	Day
Increment of time step	0.1	Dimensionless
Maximum time-step size	1.0×10^{-3}	Day

water-phase fluxes are equal to zero (boundary condition type 1 in Table 2). The bottom is assigned to Dirichlet boundary conditions of three-phase pressures (boundary condition type 5 in Table 2). Water pressure at the bottom is equal to 7.156×10^{15} g cm^{-1} day^{-2}, NAPL pressure is 7.302×10^{15} g cm^{-1} day^{-2}, and air pressure is equal to 7.465×10^{15} g cm^{-1} day^{-2}, representing water saturation and total liquid saturation equal to 0.36 throughout the simulation period. Left and right sides are no flux boundaries for all three phases. Simulation information is summarized in Table 5. The effective water saturation, NAPL saturation, and air saturation profiles at various times are indicated in Fig. 24a–c, respectively. Initially, the system is oil-free with the initial water saturation equal to 0.36 throughout the simulation domain (initial condition type 8 in Table 1). Figure 24a–c show that, as the NAPL infiltrates into the variably saturated soil column, NAPL phase displaces water and air. The displaced water forms pools just below NAPL front (NAPL and water densities are assumed the same), and air is greatly decreased in the NAPL infiltration region. Furthermore, it is observed that phase configuration changes from a water–air system to a water–NAPL–air system in the part of the simulation domain.

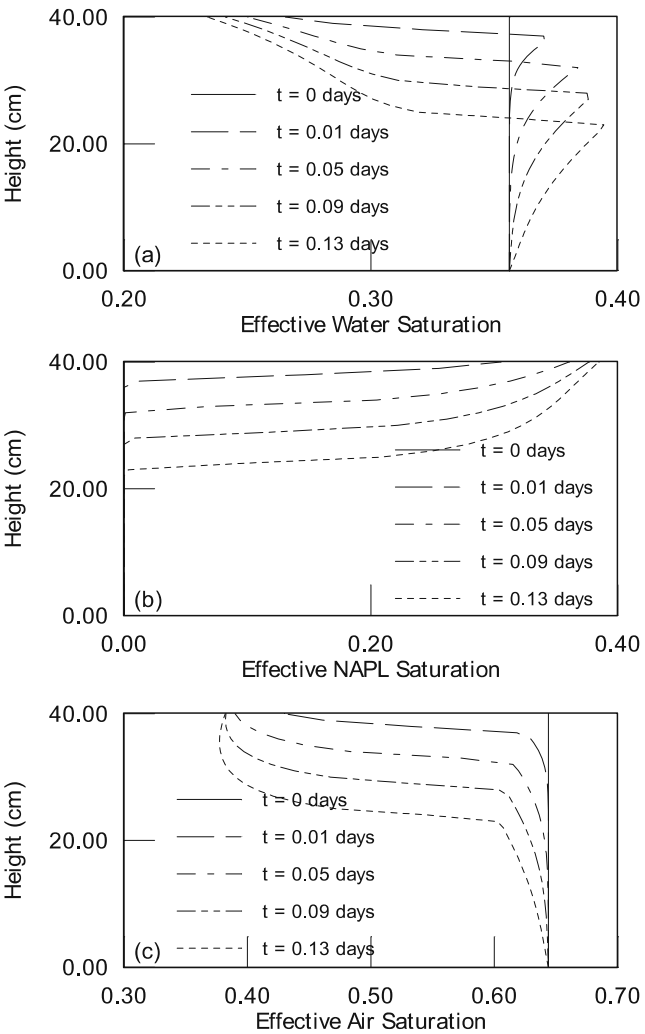

Fig. 24 Distributions of **a** water saturation, **b** NAPL saturation, and **c** air saturation at various times

5.10 DNAPL flow in physically heterogeneous media

This problem is conceptually described in Fig. 25. It is assumed that a low permeable lens is placed in the interior of the simulation region to investigate capillary pressure effects on DNAPL flow. Capillary pressure–saturation relationships after van Genuchten model [14] with different pore size distribution index, n, are assumed in the lens and surrounding matrix. The

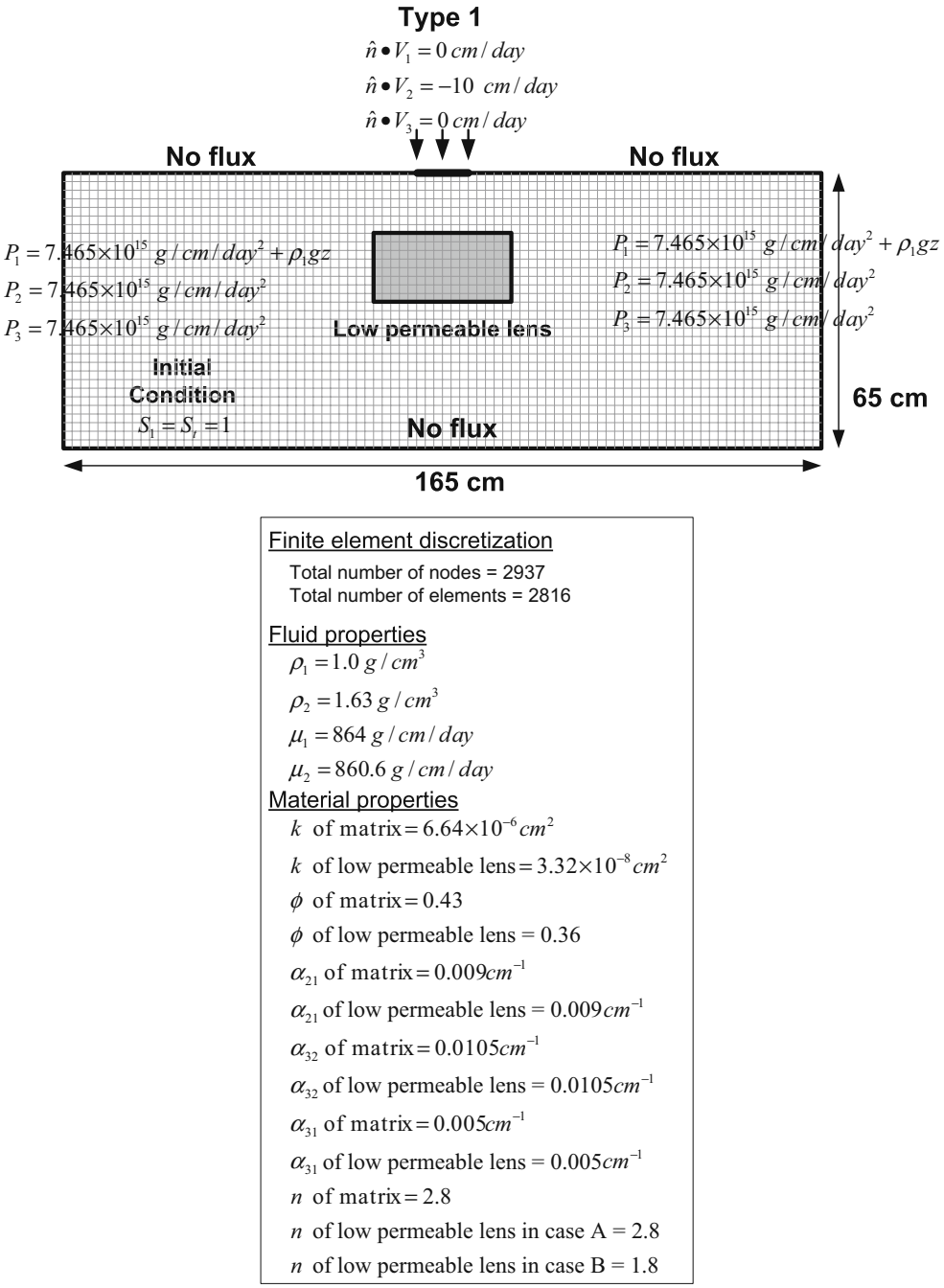

Fig. 25 DNAPL flow in physically heterogeneous media: domain of interest, initial and boundary conditions, fluid properties, material properties, and finite element discretization

bottom of the reservoir is impermeable for all three phases. Hydrostatic pressure distribution for water pressure and atmospheric pressure for gas phase are prescribed at the left and right boundaries, whereas for DNAPL phase, its pressure is prescribed such that the NAPL saturation is zero based on the van Genuchten model [14]. In other words, pressure for the DNAPL phase is equal to air pressure. Thus, boundary condition of type 5 is imposed on the left and right boundaries. At the inlet on the top boundary, a flux, 10.0 cm/day for the non-wetting DNAPL phase, is prescribed, whereas for water and air phase, no flow condition is prescribed (boundary condition type 1 in Table 2). On the remainder of the top boundary, no flux condition is imposed for all three phases. The systematic illustration of boundary conditions and conceptual model are

Table 6 Soil properties for case A and case B

Parameters	Case A		Case B	
	Matrix	Lens	Matrix	Lens
k (cm^2)	6.64×10^{-6}	3.32×10^{-8}	6.64×10^{-6}	3.32×10^{-8}
ϕ	0.43	0.36	0.43	0.36
α_{21} (cm^{-1})	0.009	0.009	0.009	0.009
α_{32} (cm^{-1})	0.0105	0.0105	0.0105	0.0105
α_{31} (cm^{-1})	0.005	0.005	0.005	0.005
n (van Genuchten fitting parameter)	2.80	2.80	2.80	1.80

indicated in Fig. 25. Initial conditions are hydrostatic pressure distribution for water, atmospheric condition for gas phase, and zero saturation for DNAPL (initial condition type 3 in Table 1). The fluid parameters are

$$\rho_1 = 1.00\ \text{g/cm}^3,\ \rho_2 = 1.63\ \text{g/cm}^3,\ \rho_3 = 1.2 \times 10^{-3}\ \text{g/cm}^3,$$
$$\mu_1 = 864.0\ \text{g cm}^{-1}\ \text{day}^{-1},\ \mu_2 = 860.6\ \text{g cm}^{-1}\ \text{day}^{-1},$$
$$\text{and } \mu_3 = 15.228\ \text{g cm}^{-1}\text{day}^{-1}$$

Relative permeability relationships and capillary pressure–saturation relationships are defined after the model of van Genuchten [14]. Two different van Genuchten parameters n for lens are assumed to investigate the effect of the capillary barrier on DNAPL flow for cases A and B. Soil properties for cases A and B are shown in Table 6. Simulation results for case A with high n are depicted in Fig. 26a, and for case B with low n in Fig. 26b. Low value of n indicates wide pore size distribution that causes lower entry pressure of non-wetting phase. It means that infiltration in the lens is possible for the lower entry pressure. As shown in Fig. 26a, it is observed that no DNAPL infiltrates the fine sand lens so the NAPL saturation is discontinuous over the lens boundary. However, in case B, DNAPL infiltration is possible, so the NAPL saturation is continuous through the lens.

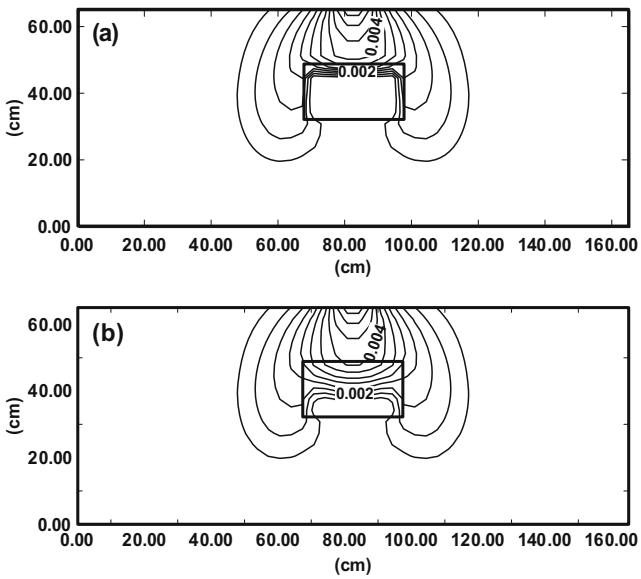

Fig. 26 DNAPL saturation plots of DNAPL infiltration for cases a and b

6 Summaries and conclusions

This paper presents the development of MPS based on a fractional-flow approach, which considers the full three-phase flows with general initial and boundary conditions. Mathematical and numerical formulations are presented. The various example problems representing a wide range of physical systems are included. Numerical strategies to deal with general boundary conditions are developed, which are usually not addressed in hydrologic literature when a fractional-flow approach is employed. The advantage of fractional-flow approaches over the pressure-based approach is shown when phase configuration change occurs in the simulation domain. The general boundary condition consists of ten cases. The first eight cases are the combinations of two types of boundaries of individual phases, flux-type and Dirichlet-type boundaries. The other two cases are the variable boundary conditions: one for water-medium interface and the other for the air-medium interface when the directions of fluxes are not known a priori. In addition, general initial conditions are eight combinations of two types of initial condition of individual phases, saturation and pressure. MPS, being a fractional-flow approach, can handle phase configuration changes without explicit assumptions often used in the traditional pressure based approaches that may produce inaccuracies in the solution.

Acknowledgements This research is supported, in part, by the National Science Foundation Grant No. EAR-0196048 with the University of Central Florida and, in part, by the US Department of Energy Grant No. DE-FG04-ER63916, with the University of Central Florida.

References

1. Bastian, P., Helmig, R.: Efficient fully-coupled solution techniques for two-phase flow in porous media parallel multigrid solution and large scale computations. Adv. Water Resour. **23**, 199–216 (1999)
2. Binning, P., Celia, M.A.: Practical implementation of the fractional flow approach to multi-phase flow simulation. Adv. Water Resour. **22**, 461–478 (1999)
3. Bradford, S.A., Abriola, L.M., Rathfelder, K.M.: Flow and entrapment of dense nonaqueous phase liquids in physically and chemically heterogeneous aquifer formations. Adv. Water Resour. **21**, 117–132 (1998)
4. Burkley, S.E., Leverett, M.C.: Mechanism of fluid displacement in sands. Trans. AIME **146**, 107–116 (1942)
5. Carrano, C.S. Jr., Yeh, G.T.: A fourier analysis of dynamic optimization of the Petrov–Galerkin finite element method. Int. J. Numer. Methods Eng. **38**, 4123–4155 (1995)
6. Celia, M.A., Binning, P.: Two-phase unsaturated flow: one dimensional simulation and air phase velocities. Water Resour. Res. **28**, 2819–2828 (1992)
7. Christie, I., Griffiths, D.F., Mitchell, A.R., Zienkiewicz, O.C.: Finite element methods for second order differential equations with significant first derivatives. Int. J. Numer. Methods Eng. **10**, 1389–1443 (1976)
8. Dekker, T.J., Abriola, L.M.: The influence of field-scale heterogeneity on the infiltration and entrapment of dense nonaqueous phase liquid in saturated formulations. J. Contam. Hydrol. **42**, 187–218 (2000)
9. Guarnaccia, J.F., Pinder, G.F.: NAPL: a mathematical model for the study of NAPL contamination in granular soils, equation development and simulator documentation. The University of Vermont, RCGRD #95-22, (1997)
10. Kaluarachchi, J.J., Parker, J.C.: An efficient finite elements method for modeling multiphase flow. Water Resour. Res. **25**, 43–54 (1989)
11. Kueper, B.H., Frind, E.O.: Two-phase flow in heterogeneous porous media, 1. Model development. Water Resour. Res. **27**, 1049–1057 (1991)
12. Kueper, B.H., Frind, E.E.: Two-phase flow in heterogeneous porous media, 2. Model application. Water Resour. Res. **27**, 1058–1070 (1991)
13. McWhorter, D.B., Sunada, D.K.: Exact integral solutions for two phase flow. Water Resour. Res. **26**, 399–414 (1990)
14. Parker, J.C., Lenhard, R.J., Kuppusamy, T.: A parametric model for constitutive properties governing multiphase flow in porous media. Water Resour. Res. **23**, 618–624 (1987)
15. Pinder, G.F., Abriola, L.M.: On the simulation of nonaqueous phase organic compounds in the subsurface. Water Resour. Res. **22**, 109S–19S (1986)
16. Sleep, B.E., Sykes, J.F.: Modeling the transport of volatile organics in variably saturated media. Water Resour. Res. **25**, 81–92 (1989)
17. Suk, H., Yeh, G.T.: 3D, three-phase flow simulations using the Lagrangian–Eulerian approach with adaptively zooming and peak/valley capturing scheme (LEZOOMPC). Hydrol. Eng. ASCE. **12**(1), 14–32 (2007)
18. van der Vorst, H.A.: Bi-CGSTAB: a fast and smoothly converging variant of Bi-CG for the solution of nonsymmetric kinear systems. SIAM J. Sci. Stat. Comput. **13**, 631–644 (1992)
19. White, M.D., Oostrom, M.: STOMP Subsurface Transport Over Multiple Phases. Theory Guide. PNL-11217. Pacific Northwest Laboratory, Richland, WA (1996)
20. Yeh, G.T., Cheng, H.P., Cheng, J.R., Short, T.E., Enfield, C.: An adaptive local grid refinement algorithm to solve nonlinear transport problems with moving fronts. In: Proc. XI-th Int. Conf. On Numerical Methods in Water Resources, pp. 577–584. Cancun, Mexico, 22–26 July, 1996 (1996)
21. Yeh, G.T., Chang, J.R., Short, T.E.: 2DFATMIC: users' manual of a two-dimensional model of subsurface flow, fat and transport of microbes and chemicals. EPA/600/R-97-052, National Risk Management Research Laboratory, U.S. EPA, Ada, OK (1997)
22. Yeh, G.T.: Computational Subsurface Hydrology Fluid Flows, 277 pp. Kluwer Academic Publishers (1999)
23. Yeh, G.T.: Computational Subsurface Hydrology Reactions, Transport, and Fate, 318 pp. Kluwer Academic Publishers (2000)